REVIEW

Metasurfaces

ADVANCED
MATERIALS

www.advmat.d

Check for
updates

From Single-Dimensional to Multidimensional Manipulation of Optical Waves with Metasurfaces

Shuqi Chen,* Zhancheng Li, Wenwei Liu, Hua Cheng, and Jianguo Tian

Metasurfaces, 2D artificial arrays of subwavelength elements, have attracted great interest from the optical scientific community in recent years because they provide versatile possibilities for the manipulation of optical waves and promise an effective way for miniaturization and integration of optical devices. In the past decade, the main efforts were focused on the realization of single-dimensional (amplitude, frequency, polarization, or phase) manipulation of optical waves. Compared to the metasurfaces with single-dimensional manipulation, metasurfaces with multidimensional manipulation of optical waves show significant advantages in many practical application areas, such as optical holograms, sub-diffraction imaging, and the design of integrated multifunctional optical devices. Nowadays, with the rapid development of nanofabrication techniques, the research of metasurfaces has been inevitably developed from single-dimensional manipulation toward multidimensional manipulation of optical waves, which greatly boosts the application of metasurfaces and further paves the way for arbitrary design of optical devices. Herein, the recent advances in metasurfaces are briefly reviewed and classified from the viewpoint of different dimensional manipulations of optical waves. Single-dimensional manipulation and 2D manipulation of optical waves with metasurfaces are discussed systematically. In conclusion, an outlook and perspectives on the challenges and future prospects in these rapidly growing research areas are provided.

1. Introduction

The functionalities of optical devices are achieved on strength of manipulating fundamental dimensions (amplitude, frequency, polarization, and phase) of optical waves in an effective way. Conventional approaches for optical waves manipulation are always related to the modulation of the optical path through a media of given refractive indices. The limited refractive indices of natural materials prevent the generation of new optical phenomena. The size and weight of traditional optical devices also prevent optical system miniaturization and integration. Nowadays, there is an ever-increasing demand for new approaches to implement the effective manipulation of optical waves in different dimensions and to get the novel optical devices on demand.

With the development of nanofabrication technology, artificial nanostructures become approachable which offer a promising solution to the achievement of efficient manipulation of optical waves in different dimensions. Metamaterials, which attain their optical functionalities from the subwavelength structures rather than their constitutive materials, provided intriguing possibilities for the evolution of modern optics and have attracted great interest from the scientific community over the past twenty years.[1–3] By judiciously modulating their subwavelength structure parameters, the effective values of the permeability and permittivity of the metamaterials can be designed on purpose to realize the manipulation of optical waves in a specific dimension and to get the desirable optical functionalities, which are even not achievable with natural materials. Previous works have demonstrated that metamaterials can be widely applied in realizing negative refractive index,[4–6] electromagnetic invisibility cloaks,[7,8] optical black holes,[9] chiral media,[10,11] and so on. However, the commercialization of metamaterial-based optical devices in real applications is still challenging, which we ascribe to the strong dispersion and high losses associated with typically used metallic structures, and also the difficult and costly fabrication for 3D designs.

Recently, planar metamaterials or metasurfaces have received great attention for their advantages to meet these challenges.[12–14] Compared to metamaterials, metasurfaces, as artificial planar designs, have dramatically reduced the fabrication complexity. Moreover, the thickness of metasurfaces is less than or similar to the wavelength of operating waves, which results in the reduction of the undesirable losses and offers an effective manner for implementing tunable and reconfigurable optical devices. Overall, metasurfaces provide an effective way to overcome the challenges in metamaterials, and it has been successfully proven that metasurfaces are more feasible for the engineering of the fundamental dimensions of optical

Prof. S. Chen, Dr. Z. Li, Dr. W. Liu, Prof. H. Cheng, Prof. J. Tian
The Key Laboratory of Weak Light Nonlinear Photonics
Ministry of Education
School of Physics and Teda Institute of Applied Physics
Nankai University
Tianjin 300071, China
E-mail: schen@nankai.edu.cn
Prof. S. Chen, Prof. H. Cheng, Prof. J. Tian
The Collaborative Innovation Center of Extreme Optics
Shanxi University
Taiyuan, Shanxi 030006, China

The ORCID identification number(s) for the author(s) of this article can be found under https://doi.org/10.1002/adma.201802458.

**ADVANCED
SCIENCE NEWS**
www.advancedsciencenews.com

**ADVANCED
MATERIALS**
www.advmat.de

waves.[15–20] Nowadays, metasurfaces can be readily fabricated using mature nanofabrication technologies, such as nanoimprint lithography, direct laser written, electron beam lithography, and ion beam etching.[15] The further involving of new constituent materials (such as dielectric, phase change material, and 2D material) and new design methods (such as few-layer metasurfaces, Huygens' metasurfaces, and folding metasurfaces) provide additional degrees of freedom for optical wave manipulation with metasurfaces, which enable the realization of multidimensional manipulation of optical waves.[12–40] Particularly, 2D manipulations of optical waves with metasurfaces in recent works have greatly extended the application scope of metasurfaces, as shown in **Figure 1**a. The realization of optical wave manipulation with metasurfaces results in numerous novel applications and ultrathin optical devices, which indicate a bright future of the real applications of metasurfaces in nanophotonics.

Here, we review the recent advances from single-dimensional to multidimensional manipulation of optical waves with metasurfaces, which are practically important and widely concerned on this research area. We provide a classification of recent works from the viewpoint of different dimensional manipulations of optical waves and also show the development trend of metasurfaces for effective dimensional manipulation of optical waves, as shown in Figure 1b. This article is organized into three main sections. In Section 2, we discuss the metasurfaces for single-dimensional manipulation of optical waves. The metasurfaces for 2D manipulation of optical waves are further discussed in Section 3. An outlook presenting our opinions on challenges and future prospects in multidimensional manipulation of optical waves is provided in the last section.

2. Single-Dimensional Manipulation of Optical Waves with Metasurfaces

Realizing effective manipulation of the amplitude, polarization, phase, and frequency of optical waves respectively is the main and fundamental research area for metamaterials and metasurfaces in the past decade. With effective manipulation of optical waves in these fundamental dimensions, metasurfaces based on metallic, dielectric, and reconfigurable materials have been widely used to realize ultrathin optical devices and novel optical phenomena. In this section, typical approaches in recent years for single-dimensional manipulation of optical waves with metasurfaces are briefly discussed.

2.1. Manipulating Amplitude of Optical Waves

Modulating the absorption, transmission, and reflection intensity of optical waves is a fundamental requirement for numerous optical applications, which is a main part of early research in artificial nanostructures.[1–3] Among the numerous research branches in this area, metamaterial absorber is one of the most important for its wide applications in sensors, thermal imaging, and so on.[21] Since its first experimental demonstration, perfect absorption in artificial nanostructures has been widely studied in the past decade.[41–55] Up to now, perfect metamaterial

Shuqi Chen is a professor at the Key Laboratory of Weak Light Nonlinear Photonics, Ministry of Education, School of Physics and Teda Institute of Applied Physics, Nankai University, China. He received his joint training Ph.D. degree from the University of Arizona, USA, and Nankai University, China, in 2009. His current research interests include nonlinear optics, phononics and acoustics metasurfaces, and subwavelength electromagnetics.

Zhancheng Li is a post-doctoral research associate at the Key Laboratory of Weak Light Nonlinear Photonics, Ministry of Education, School of Physics and Teda Institute of Applied Physics, Nankai University, China. He received his bachelor's degree in materials physics from Nankai University in 2013. His current research focuses on chiral metasurfaces.

Wenwei Liu is a post-doctoral research associate at the Key Laboratory of Weak Light Nonlinear Photonics, Ministry of Education, School of Physics and Teda Institute of Applied Physics, Nankai University, China. He received his bachelor's degree in theoretical physics from Nankai University in 2013. His current research focuses on dielectric metasurfaces.

absorbers with polarization insensitive and wide angle optical response have been well proposed in multi and broad bandwidth to meet the requirements for their real applications.[46–55] For example, Chen et al. demonstrated a broadband near perfect metamaterial absorber in near infrared.[46] Absorption with over 80% efficiency was experimentally obtained in the range of 2850–3260 nm. Recently, perfect absorbers based on metasurfaces provide a new direction for related research area.[56–58] Li et al. proposed a novel metasurface absorber which can realize bidirectional perfect absorption in 1352 nm (**Figure 2**a–c).[57] The physical mechanism of previous metamaterial absorbers is to minimize the transmission and reflection intensity of
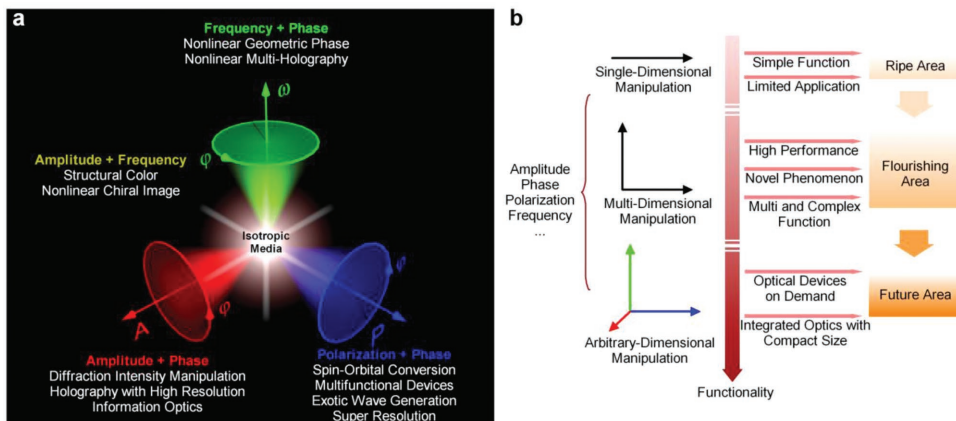
Figure 1. a) Overview of the applications associated with 2D manipulation of optical waves. b) The development trend of metasurfaces for effective manipulation of optical waves.
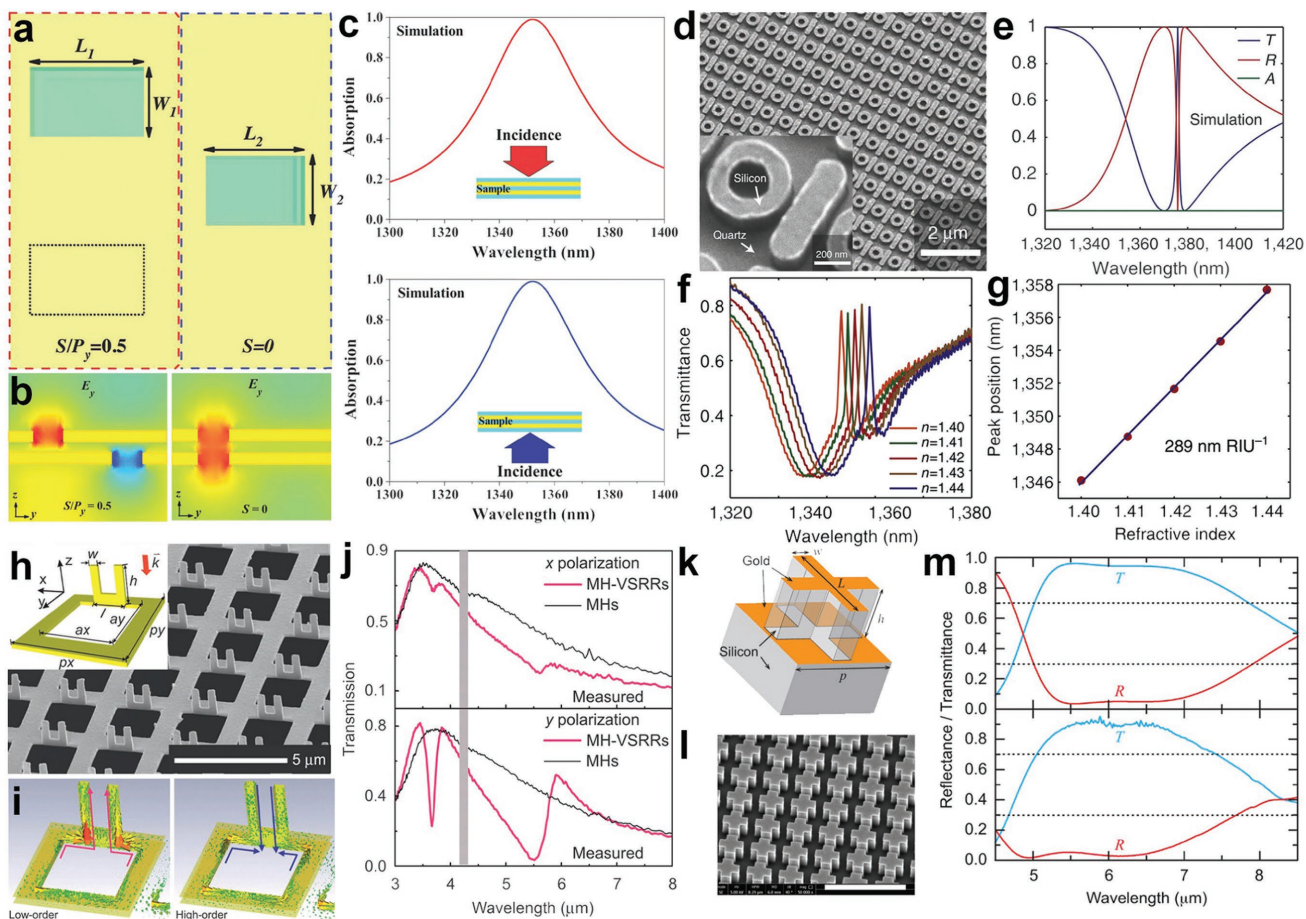
Figure 2. a) Schematics of the unit cell of the metasurface bidirectional absorber. b) Simulated E_y patterns for the aligned and separated nanoapertures. c) Simulated absorption spectra of the bidirectional absorber for incident optical waves propagating in two opposite directions. d) Scanning electron microscopy (SEM) image of the Si-based metasurface. e) Simulated transmission (T), reflection (R), and absorption (A) of the Si-based metasurface. f) Measured transmission of the Si-based metasurface with the refractive index in the range from 1.40 to 1.44. The metasurface was immersed in oil. g) The position of the resonance peak in f) when varying the background refractive index. h) SEM image of the 3D metasurface and the schematic of one unit cell. i) Simulated current distributions of one unit cell of the 3D metasurface at the low-order and high-order resonance dips in (j). j) Measured transmission of the designed 3D metasurface shown in (h) under normal x- and y-polarized incidences, respectively. k) Unit cell schematic of the bilayer metasurface. l) Large-scale view of the mid-infrared design. m) Simulated (top half) and measured (bottom half) reflection and transmission spectra. a–c) Reproduced with permission.[57] Copyright 2017, Wiley-VCH. d–g) Reproduced with permission.[64] Copyright 2014, Nature Publishing Group. h–j) Reproduced with permission.[65] Copyright 2015, Nature Publishing Group. k–m) Reproduced with permission.[76] Copyright 2017, American Chemical Society.

**ADVANCED
SCIENCE NEWS**
www.advancedsciencenews.com

**ADVANCED
MATERIALS**
www.advmat.de

optical waves simultaneously by reasonably tailoring the electric and magnetic response of their subwavelength structures. Different from these previous designs based on metamaterials, the proposed metasurface absorber minimizes the transmission and reflection intensity of optical waves by transforming incident optical waves into evanescent waves. The proposed absorber consists of two pairs of nanoapertures (Figure 2a), the bottom and top nanoapertures are aligned or separated along the y-direction. Through this special alignment design, a large phase gradient can be introduced along the metasurface interface (Figure 2b), which leads to the generation of surface evanescent waves. Because the unit cell of the proposed design is symmetric for two opposite directions, the absorption is bidirectional (Figure 2c). Moreover, the bidirectional absorption in this novel design is irrelevant to the coherence of the optical waves, and can increase the absorption capacity by 100% compared with a conventional metasurface absorber, which largely expands and improves the optical properties of metamaterial absorbers. Instead of using metallic structures, Fan et al. recently demonstrated an all-dielectric metasurface absorber for imaging through terahertz (THz) to infrared waveband.[58] Incident THz waves can be strongly absorbed solely within the cylindrical resonators, and can further be converted to heat. With the proposed all-dielectric metasurface absorber, an uncooled infrared camera can be utilized to achieve diffraction-limited imaging at THz frequencies. These results indicate that the involving of new design mechanisms and new materials will further expand the real applications of metasurface absorbers in solar cell and thermal imaging.

Fano resonances in metasurfaces, which result in narrow transmission or reflection window, have also got a great deal of attention recently for their wide applications in biosensing, slow light, optical switching, and enhancing nonlinear interactions.[59–66] The optimization of Q factor and intensity of the Fano resonances plays a key role in the real applications of Fano resonances.[67,68] Fano resonance with Q factor higher than 10^4 has been experimentally demonstrated in gigahertz (GHz) with a metallic metamaterial.[69] However, ascribing to the significant dissipation losses, it is very challenging to realize Fano resonances with high Q factor in optical wavebands by using metallic nanostructures.[70] Recently, dielectric nanostructures have been widely utilized to achieve high Q factor Fano resonances in optical wavebands.[64,71–73] Yang et al. utilized Si-based metasurfaces to experimentally demonstrate a sharp transmission window in the near-infrared regime (Figure 2d–g).[64] A transmission window with 82% peak intensity was achieved in near-infrared with a high Q factor of 483 (Figure 2e). The high Q factor is attributed to the coherent interaction among the subwavelength resonators in the proposed design that results in the minimization of both nonradiative and radiative damping. This design can be used as a refractive index sensor with high sensitivity of 289 nm per RIU, whose performance far exceeded previous designs based on Fano resonance (Figure 2f,g). A recent theoretical approach further indicates that the Q factor of Fano resonances in optical wavebands can reach 10^5 with dielectric metasurfaces.[73] Instead of using dielectric nanostructures, some new approaches based on novel metallic designs have also been proposed in optical wavebands for the realization and application of Fano resonances. Cui et al.

proposed a novel 3D single-layer folding metasurface to realize unusual and well-scalable Fano resonances (Figure 2h–j).[65] The realization of Fano resonance in the proposed design is attributed to the presence of a 3D hybridization in current flow. As show in Figure 2i, the current flows of the low-order and the high-order modes exhibit a 3D route and the currents flowing in z direction are parallel and antiparallel to the currents flowing in x–y plane, respectively. The resonance modes associated with the vertical current flows are unique "dark" modes, which cannot be directly excited by normal incident waves. The excitation of these "dark" modes in the proposed folding metasurfaces is attributed to the 3D hybridized currents flowing between the vertical U-shaped resonators and the horizontal rectangular holes, which appears to be unique to the folding designs and has not been reported for any traditional metamaterials or metasurfaces. The unusual Fano resonances in the proposed design provide new possibilities for real applications of metasurface in biosensing and imaging.[65,66] In a recent research, metasurface also shows its great ability on the modulation of the reflection and transmission intensity of optical waves in a broad bandwidth.[74–76] Huang et al. showed that dual and broadband optical antireflection can be realized in the mid-infrared and THz bandwidths by using bilayer metasurfaces (Figure 2k–m).[76] The broadband antireflection is due to the similar reflection amplitude and opposite phase dispersion of the two layers of the metasurfaces. This design principle provides a practical guidance for bandwidths expansion of optical antireflection and the designing of future broadband metasurface.

2.2. Manipulating Phase of Optical Waves

Since phase is the most basic characteristic that reveals light is a kind of wave, the manipulation of phase always draws attention of the scientific community. Even the manipulation of polarization can be realized using phase modulation, such as waveplates. In tradition, the phase of optical waves is modulated through the optical path when light travels in media, such as birefringent crystals, with applications of lenses, phase masks, holography, and so on. However, crystals based phase manipulation suffers from chromatic dispersion and bulky size, which limit the realization of integrated optical systems and further information transmission. In the past decade, the burgeoning development of subwavelength nanoantennas makes it convenient to manipulate phase in micrometer or nanometer scale. Yu et al. proposed generalized law of reflection and refraction, with a discontinuous phase gradient aligned in an ultrathin surface (about 50 nm with incident wavelength of 8 µm).[77] As shown in **Figure 3**a, a V-antenna simultaneously supports symmetric and antisymmetric resonant modes, resulting in a phase modulation from 0 to π.[77–79] On the other hand, a mirror-symmetric V-antenna will introduce a π phase change, which can further expand the phase modulation from 0 to 2π. Since the building block of metasurfaces is at the subwavelength scale, and the thickness is about $\lambda/100$,[77–81] metasurfaces enable us to manipulate the wavefront in a single surface. One of the intriguing applications of the phase modulation is anomalous refraction (Figure 3b), the
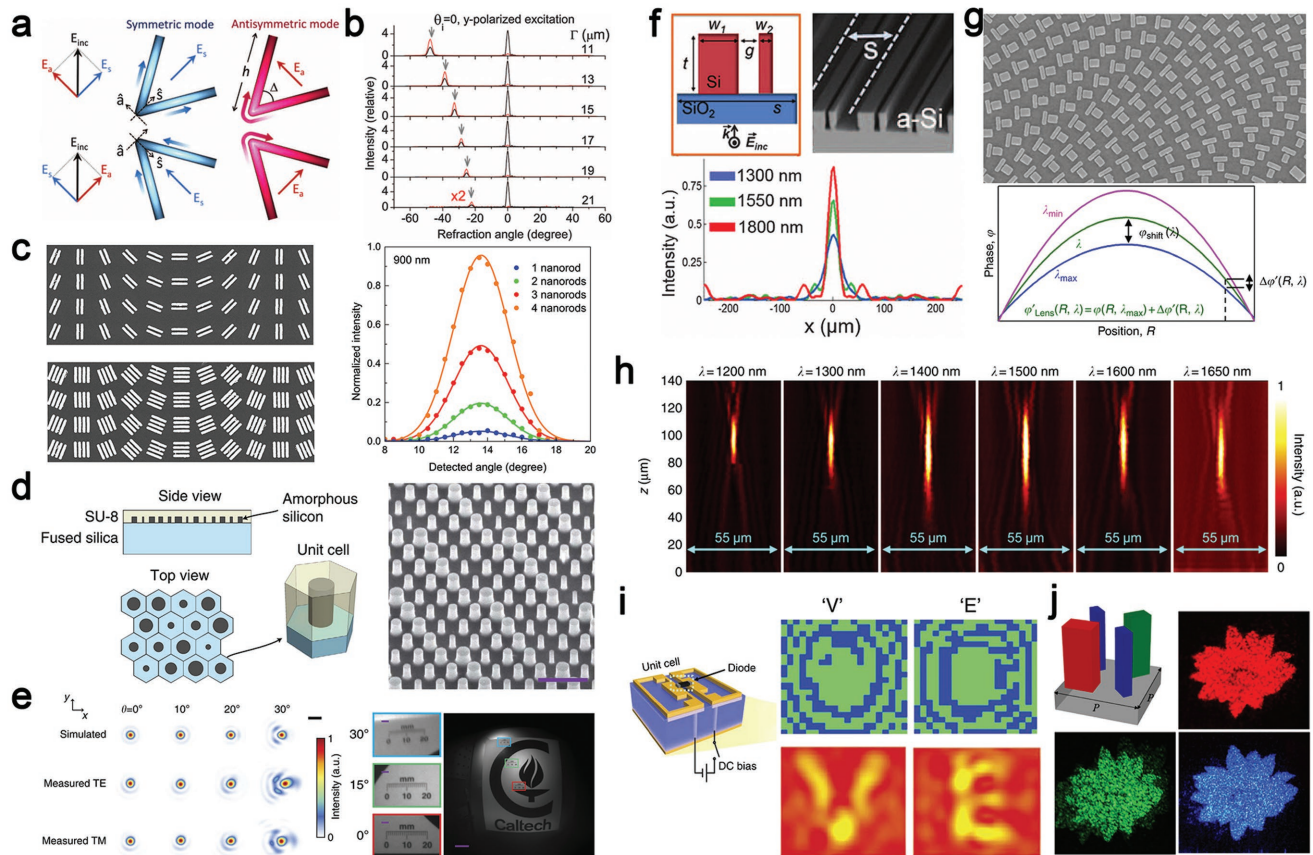
Figure 3. a) A V-antenna supporting symmetric and antisymmetric modes can be utilized as the building block of discontinuous phase modulation. By varying the geometric size and arrangement of V-antennas, the antennas can scatter light with a phase range from 0 to 2π. b) The anomalous light can be refracted to other directions when the V-antennas are aligned with a linear phase gradient (red lines). c) An SEM image of the geometric phase based gold antennas. The phase of the scattered anomalous light is proportional to the rotational angle of the antenna under local coordinate. The efficiency of the refracted light increases when the number of nanorods increases due to eigenstates coupling. d) Schematic and the SEM image of the dielectric metasurface which employs the doublet configuration to correct aberrations. e) Simulated and measured focal plane intensity profiles with incident angles from 0° to 30°. An integrated camera is realized with the metasurface doublet lens, the size of which is only 1.6 mm × 1.6 mm × 1.7 mm. f) Multiwavelength achromatic metasurfaces realized by silicon waveguides. By changing the width of the waveguides, the phase difference of propagation can be compensated by the resonant phase, leading to the achromatic behavior in three separate wavelengths. g) An SEM image of the broadband achromatic metasurface. Inset: Phase profile for the broadband achromatic metasurface at arbitrary wavelength of $\lambda \in \{\lambda_{min}, \lambda_{max}\}$. By gathering both geometric and resonant phases, the dielectric building block can realize the designed achromatic phase distribution in the working waveband. h) The measured intensity profiles show that the metasurface can achromatically focus the incident light from 1200 to 1680 nm. i) Reprogrammable metasurface holograms realized by two metallic loops with a pin diode welded in between that can be controlled by a direct current voltage. The binary phase and measured intensity profiles of the coding metasurface for different holographic images of "V", and "E". j) Multiwavelength achromatic and highly dispersive holograms realized by dielectric building blocks in the visible regime. The three-primary colors (red, green, blue) holograms are experimentally observed. a,b) Reproduced with permission.[77] Copyright 2011, American Association for the Advancement of Science. c) Reproduced with permission.[91] Copyright 2015, Wiley-VCH. d,e) Reproduced with permission.[99] Copyright 2016, Nature Publishing Group. f) Reproduced with permission.[103] Copyright 2015, American Association for the Advancement of Science. g,h) Reproduced with permission.[109] Copyright 2017, Nature Publishing Group. i) Reproduced with permission.[112] Copyright 2017, Nature Publishing Group. j) Reproduced with permission.[113] Copyright 2016, American Chemical Society.

incident light can be refracted to another direction following the generalized law of refraction. Other nanostructures are also investigated to control optical phase based on different resonant modes.[82–87] Another distinguished way of phase modulation is Pancharatnam–Berry phase, which is basically a topological characteristic regarding polarization.[88,89] The phase of the anomalous light (with polarization perpendicular to the incident circularly polarized light) ϕ is proportional to the orientation angle θ, i.e., $\phi = 2\sigma\theta$, where $\sigma = \pm 1$ is the spin angular momentum of the incident light.[90] This method makes it easier to determine the exact phase value by simply controlling the orientation angle of the nanostructure. Moreover, the scattering strength remains the same, since the rotated nanostructure seems the same to a circularly polarized light in a local coordinate. Liu et al. proposed multirod building blocks to improve the efficiency of Pancharatnam–Berry phase (Figure 3c) up to 25% (theoretical limitation for polarizer based Pancharatnam–Berry phase).[91] Recently, the revolutionary development of dielectric metasurfaces highly improves the efficiency of metasurfaces (about 100%), resulting from the ability of dielectric nanoparticles to simultaneously stimulate electric and magnetic dipole/multipole

ADVANCED
SCIENCE NEWS
www.advancedsciencenews.com

ADVANCED
MATERIALS
www.advmat.de

resonances.[92–94] By designing the phase distribution of a metasurface, a metalens can be achieved in a compacted size.[95–97] Khorasaninejad et al. proposed a diffraction-limited metalens at visible wavelengths, with smaller focusing full-width at half-maximum than a commercial objective.[98] Arbabi et al. proposed a miniature planar optical camera based on doublet corrected dielectric metalens, with a total size of 1.6 mm × 1.6 mm × 1.7 mm, including the metalens and a complementary metal-oxide-semiconductor (CMOS) detector (Figure 3d,e).[99]

One of the most challenging problems in optics is chromatic aberration, which results from different phase accumulations for varied incident wavelengths. Actually, the concept achromatism is strongly related to the functionality of the device to be implemented. For example, if the phase of each unit cell is wavelength-independent, such as Pancharatnam–Berry phase,[91] the achromatic functionality of the device can be realized by local broadband design without considering the propagation of light in free space.[100–102] However, for other devices that involve the propagation properties of light, such as metalens, the chromatic aberration is more complicated. Aieta et al. proposed achromatic metasurfaces design by dispersive resonant phase compensation based on dielectric materials (Figure 3f). With delicate design of silicon waveguides, an engineered wavelength-dependent phase shift can be achieved to compensate the propagation phase differences for three separate wavelengths.[103] Later on, the same group reported another achromatic metalens at telecommunication wavelengths.[104] Recently, several methods of achromatic realization have been proposed,[105,106] and the most exciting ones are broadband achromatic metasurfaces.[107,108] As shown in Figure 3g,h, Wang et al. realized achromatic metasurface over a broadband wavelength region from 1200 to 1680 nm, working in a reflection scheme.[109] By combining resonant and Pancharatnam–Berry phases, the metasurfaces are able to provide the accurate phase profile as the ideal requirement for broadband achromatic flat devices. Since phase can be arbitrarily controlled at the subwavelength scale, holography can also be realized in the metasurfaces platform.[110,111] Li et al. proposed an electromagnetic reprogrammable coding metasurface that can display different hologram frames by controlling the digital current voltage of each unit cell (Figure 3i).[112] The unit cell size is 6 mm × 6 mm × 2 mm working at the frequency of 7.8 GHz. However, the reprogrammable metasurface in infrared and optical regime is still challenging because the unit cell will be much smaller, making it difficult to independently control the phase of each unit cell. Dielectric holograms are also proposed to improve the efficiency.[113,114] As shown in Figure 3j, the silicon metasurfaces composed of three kinds of nanoblocks can manipulate wavefront of incident light with different colors. These researches significantly expanded the applications of metasurfaces phase modulation.

2.3. Manipulating Polarization of Optical Waves

The polarization state manipulation with metasurfaces always involves the tailoring of the anisotropic wave interference at the subwavelength scale. By manipulating the amplitude and phase of the electric or magnetic components in two orthogonal directions, the polarization state of light can be altered with structures occupying two orthogonal resonances, including elliptical nanoholes, L-shaped nanoparticles, crossed nanodipoles.[115–120] Among the abundant polarization devices, waveplates play a crucial and fundamental role in modern optical and photonic applications such as sensing, imaging, and communication. Liu et al. proposed a method of designing half-wave plate with anisotropic metallic nanoantenna pairs.[121] As shown in **Figure 4**a, the nanoantennas in the first/second row rotate clockwise/counterclockwise along the x-axis. The angular bisector of the nanosturcture pairs remains unchanged for different rotation angles, making the metasurfaces possess a constant optical axis. The measurements in Figure 4b,c show that a phase difference of π/2 is achieved for two orthogonal direction, and the rotated polarization of an angle π/2 is also realized. Another method of rotating polarization by π/2 is based on near-field interference, which eliminates the parallel electric component and reserves/enhances the orthogonal electric one.[122,123] Wu et al. proposed S-shaped holes in a silver film (Figure 4d) that can simultaneously excite surface plasmon polaritons and localized surface plasmons. With superposition of the two resonances, the electric component parallel to the incident polarization is restrained, and the vertical electric component is enhanced, leading to an orthogonal polarization conversion with ellipticity as low as 0.0078.[123] Moreover, the polarization rotation angles increase when changing the thickness of the sample (Figure 4e). Yu et al. realized a broadband quarter-wave plate using V-antennas (Figure 4f). With linear polarization incidence, the subunits produce two copropagating waves with the same strength, orthogonal linear polarization state, and a π/2 phase contrast.[124] Thus, a circularly polarized extraordinary output beam is realized. The phase difference remains π/2 and the ratio of amplitude for perpendicular polarization remains unitary from 5 to 12 μm. Such kind of metasurface-based waveplates employ arrays of anisotropic nanostructures that can generate two orthogonal eigenmodes, which extremely limited the working waveband (Figure 4g). On the other hand, the efficiency of such waveplate is only about 10%.

As mentioned in the previous parts, metasurfaces provide an extraordinary platform for enhancing the light–matter interaction, which mainly originates from the abundant near-field effects supported by subwavelength nanoparticles. Yu et al. proposed a giant optical activity without chiral structures working in the near infrared waveband,[125] as shown in Figure 4h–j. The controllable optical activity is attributed to the phase difference of the two orthogonal circularly polarized components decomposed from the linearly polarized light. The cross-shaped nanostructure can convert the linearly polarized light into left circularly polarized (LCP) or right circularly polarized (RCP) light, with a phase difference that controls the polarization angle of the output light. The experimental results show that the polarization of the transmitted light is nearly linearly polarized. Other polarization manipulation has also been realized,[126–133] with different kinds of materials and designing principles. Compared with the low efficiency of plasmonic polarization modulation, dielectric metasurfaces can manipulate polarization with unitary efficiency,

ADVANCED
SCIENCE NEWS
www.advancedsciencenews.com

ADVANCED
MATERIALS
www.advmat.de
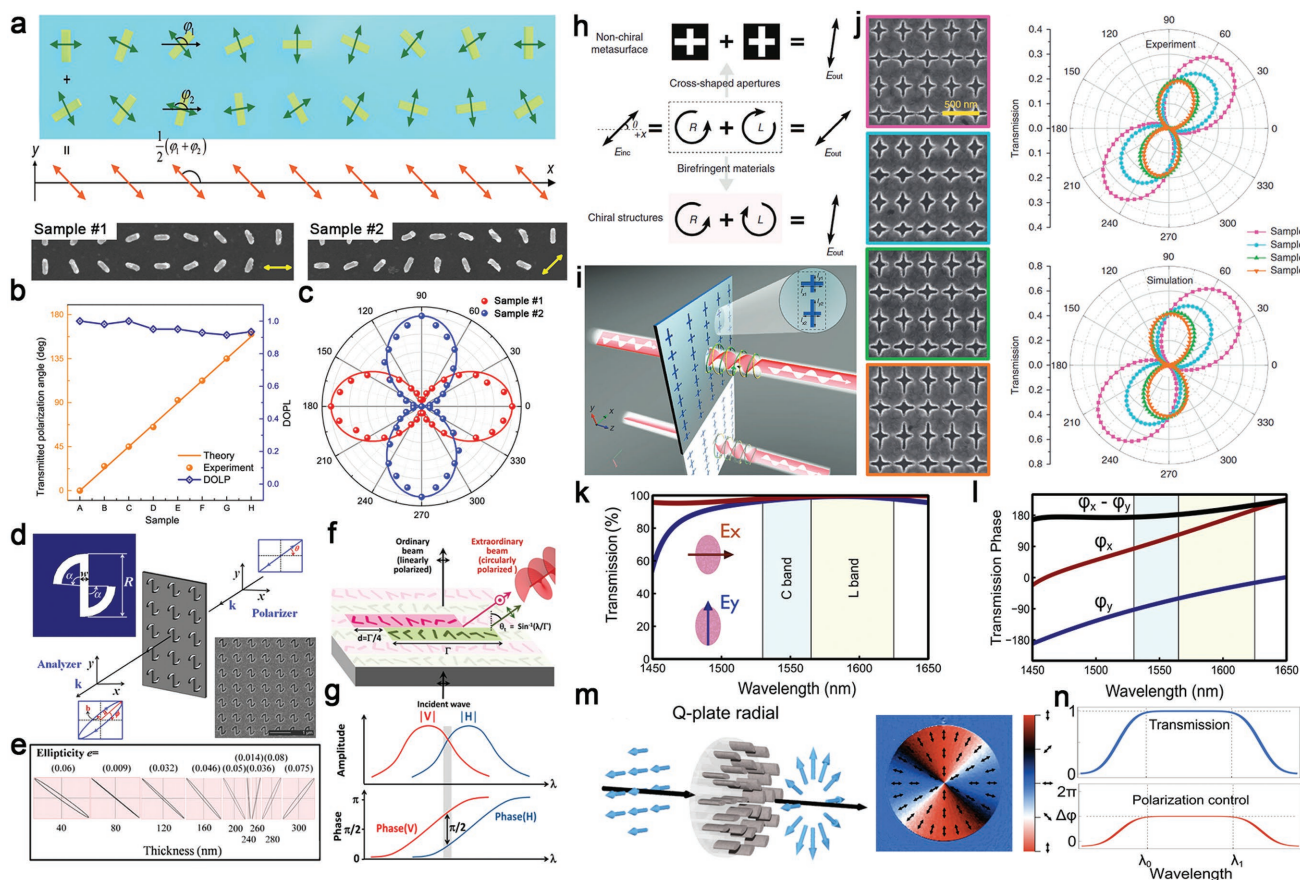
Figure 4. a) The superunit cells consist of anisotropic metal nanoantenna pairs. The top/bottom row nanoantennas rotate in the clockwise/counterclockwise direction. The orange arrows show the bisection angle of the nanoantenna pairs $(\phi_1 + \phi_2)/2$ and the optical axis of the half-wave plate. b) Theoretical and measured polarization angle of the image light for different incident polarization angles at wavelength 980 nm. The orange line indicates an ideal half-wave plate as comparison. c) Measured transmission intensity through an analyzer for samples #1 (red) and #2 (blue). d) Schematic of the experimental setup of the single layer polarization rotator. The incident polarization is long in the x direction. e) The polarization states of the transmitted light with different thicknesses of the metasurfaces. f) Broadband quarter-wave plate plasmonic metasurface, which consists of two subunits (pink and green) with each containing eight different V-shaped gold antennas. The two subunits generate x- and y-polarized light with a phase difference of $\pi/2$. g) Conventional plasmonic quarter-wave plate metasurfaces are based on antennas that support two orthogonal eigenmodes, which only functions in a narrow waveband range (gray area). h) The nanocrosses hollow with different geometric sizes can convert incident linearly polarized light into right/left circularly polarized light with a phase difference. The interference of these two opposite circularly polarized light results in a linearly polarized one with the orientation rotated compared with the incident polarization. i) Schematic of the interference process when light passes the metasurface. j) Simulated and measured intensity of the output light with four designed metasurfaces. k) The transmission of the designed dielectric metasurface for two orthogonal polarization approaches one (high efficiency). l) The phase difference for the two directions is around π, indicating this metasurface can serve as a broadband half-wave plate. m) Illustration of the generation of vector beam with dielectric building blocks. n) Broadband achromatic dielectric metasurfaces for polarization control. a–c) Reproduced with permission.[121] Copyright 2017, American Chemical Society. d,e) Reproduced with permission.[123] Copyright 2013, American Physical Society. f,g) Reproduced with permission.[124] Copyright 2012, American Chemical Society. h–j) Reproduced with permission.[125] Copyright 2016, Nature Publishing Group. k–n) Reproduced with permission.[137] Copyright 2016, American Institute of Physics.

and the controlled polarization may cover the whole Poincaré sphere.[134–136] Kruk et al. proposed high ratio silicon nanopillars based on the generalized Huygens' principle.[137] They experimentally demonstrated that the transmission reaches 90% and polarization conversion efficiency of ≈99% can be obtained in the telecommunication wavebands (Figure 4k,l). Moreover, the metasurface remains its functionality over a broad spectral range, without sacrificing its high efficiency. This design methodology not only can be utilized to achieve a waveplate, other polarization modulation such as vector beam generation can also be accomplished (Figure 4m).

Furthermore, by choosing other high-index transparent dielectric materials, the results presented can be easily introduced to other wavebands (Figure 4n). To date it is still challenging to realize full control of polarization across an ultra-broadband wavelength range, which may require revolutionary development of design strategies, since the resonance based design usually has specific working wavelengths. With the development of metasurface fabrication technology, metasurface devices for polarization state manipulation are expected to have deep impact on modern photonic applications and integrated microoptics systems.

ADVANCED
SCIENCE NEWS
www.advancedsciencenews.com

ADVANCED
MATERIALS
www.advmat.de

2.4. Manipulating Frequency of Optical Waves

Since its first introduction, metasurfaces have been successfully utilized to realize many novel applications and new phenomena in linear optics. Recently, with the increasing demand for the integrated multifunctional devices in optical communication, frequency manipulation of optical waves with metasurfaces or the nonlinear properties of metasurfaces have received considerable and growing attention.[22,27,36] In conventional nonlinear crystals, phase matching condition needs to be satisfied in nonlinear processes for the achievement of high efficient nonlinear optical generation.[138] Compared with conventional nonlinear crystals, the requirement of phase matching condition is relaxed in metasurfaces because the nonlinear processes only occur in a thin layer with subwavelength thickness. The strong field enhancement near the surface which leads to strong light–matter interaction results in the efficient nonlinear optical processes in metasurfaces.[36,139]

Efficient second harmonic generation (SHG) has been well studied in metasurfaces with metallic structures.[140–147]

Because the nonlinear processes of SHG in metasurfaces must be treated as scattering phenomenon instead of a phase-matched one, phase matching condition is substituted with mode matching condition in metasurfaces.[144–147] Numerous designs with multiresonances have been proposed to improve the efficiency of SHG. Celebrano et al. experimentally realized an enhanced SHG in multiresonant plasmonic nanoantennas (**Figure 5**a–c).[147] The realization of this intense SHG is attributed to the simultaneous utilization of multiple plasmonic resonances, axial symmetry broken, and spatial mode overlap at the nanoscale. Compared to single resonant V-shaped antenna, the peak intensity for second harmonic wave is two times higher in the proposed multiresonant plasmonic nanoantenna with the resonance of rod matching the second harmonic wavelength.

Because metasurfaces with metallic structures generally suffer from large optical absorption and low melting temperature, metasurfaces with dielectric structures are widely used to enhance the third harmonic generation (THG) in recent years.[148–153] Yang et al. utilized a Fano resonance based silicon
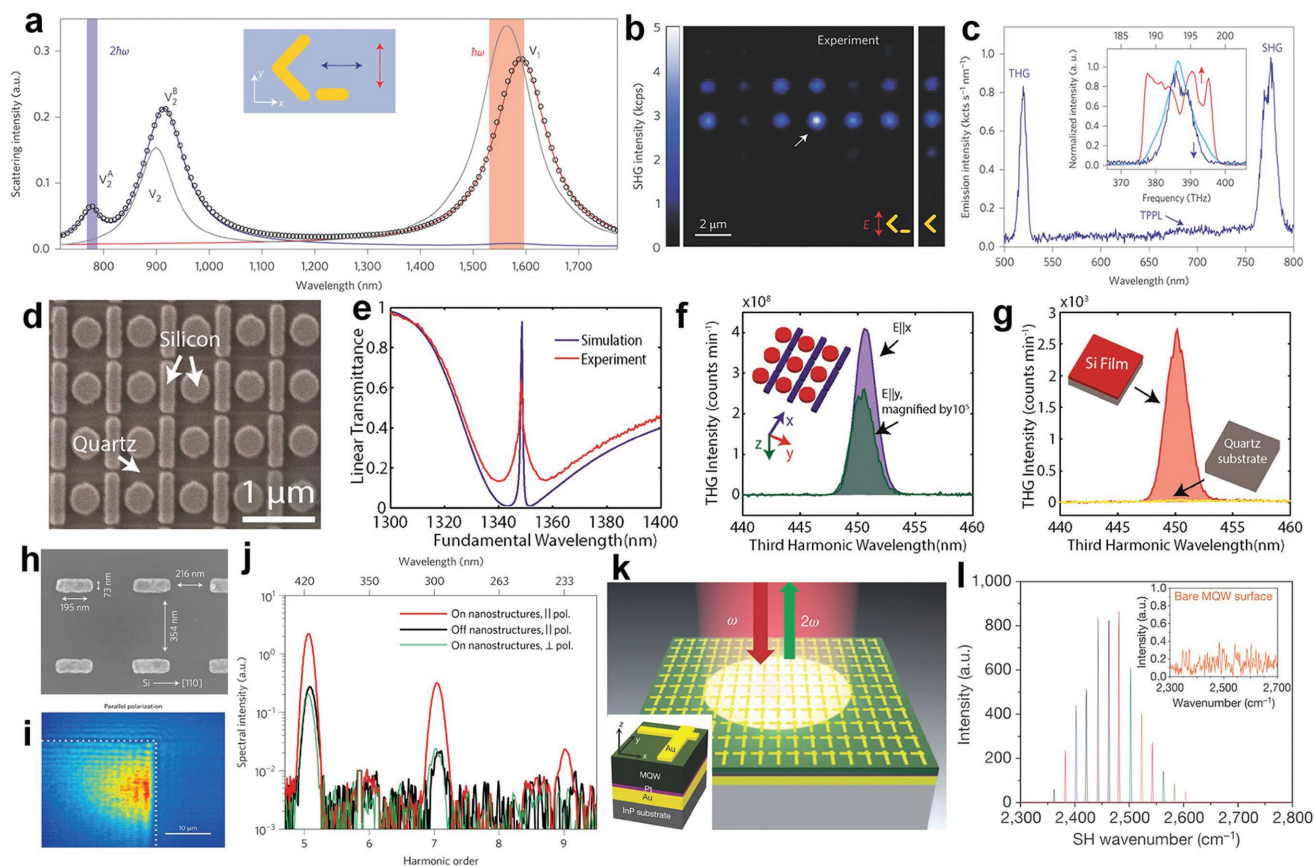
Figure 5. a) Scattering spectra of the V-shaped antenna (grey line) and the coupled antenna (black circles). b) SHG intensity for the array of the coupled antenna and isolated V-shaped structures with different geometric parameters. c) Emission intensity of the coupled antenna. d) SEM image of the Si-based nonlinear metasurface. e) Simulated and measured transmission spectra. f) THG intensity with x- and y-polarized fundamental incidences, respectively. g) THG intensity of an unpatterned Si film and a bare quartz substrate, respectively. h) SEM image of the nanoantenna array. i) Image with the 5th harmonic of a corner of an illuminated array. j) High-harmonic intensity with the polarization of illumination parallel and perpendicular to the major axis of the antennas. The blackline is the emission from bulk Si. k) Schematic of the hybrid metasurface and a diagram of one unit cell. l) Spectra of second harmonic output for different pump wavenumbers. a–c) Reproduced with permission.[147] Copyright 2015, Nature Publishing Group. d–g) Reproduced with permission.[153] Copyright 2015, American Chemical Society. h–j) Reproduced with permission.[156] Copyright 2017, Nature Publishing Group. k,l) Reproduced with permission.[159] Copyright 2014, Nature Publishing Group.

**ADVANCED
SCIENCE NEWS**

www.advancedsciencenews.com

**ADVANCED
MATERIALS**

www.advmat.de

metasurfaces to realize efficient THG with enhancement improvement of 1.5×10^5 with respect to an unpatterned silicon film (Figure 5d–g).[153] The enhanced THG is attributed to the local electric field enhancement within Si which is induced by the high Q factor Fano resonance.

Metasurfaces have also been used for efficient four-wave mixing processes and high-harmonic generation.[154–156] Vampa et al. adopted nanoantenna arrays to demonstrate plasmon-assisted high-harmonic generation (Figure 5h–j).[156] With nanoantenna array on top of the substrate, the high-harmonic emission is several times stronger than that without the antennas. This enhanced high-harmonic generation is attributed to the polarization-dependent local field enhancement, which occurs only when the polarization of the incident laser is parallel to the antennas, as shown in Figure 5i.

For the generation of giant nonlinear response, hybrid metasurfaces consist of plasmonic metasurfaces and materials with large nonlinear optical responses have also been proposed.[157–159] With the combination of plasmonic metasurfaces and semiconductor heterostructures, Lee et al. realized a record-high SHG (Figure 5k,l).[159] A power conversion efficiency of almost 2×10^{-26} using a pump intensity of only 15 kW cm^{-2} was experimentally demonstrated. The giant SHG can be attributed to the strong modal overlap between the fundamental and second harmonic modes in the nanostructures and the effective tailoring of the near-field polarizations. This design principle provides an effective way for the realization of giant nonlinear response in metasurfaces. The further implementation of giant nonlinear response in metasurfaces will greatly boost the applications of metasurfaces in nonlinear optics and pave the way for multidimensional manipulation of optical waves.

2.5. Dynamic Manipulation of Optical Waves in 1D

Realizing the dynamic manipulation of optical waves, which is a fundamental requirement of optical integration, plays a key role in optical switch, optical communication, and the implementation of optical multifunctional devices.[26,28] Nowadays, the dynamic manipulation of optical waves with metasurfaces always involves reconfigurable materials or elastic substrates.[160–175] For example, varactor diodes, flexible substrate, and liquid metals are widely used in GHz to realizing the dynamic manipulation of electromagnetic waves, while semiconductor, superconductor, perovskite, and 2D materials are main approaches in THz regime.[160–167] To realizing the dynamic manipulation of optical waves, phase change materials, 2D materials, liquid crystal, and elastic substrates are normally used.[168–175]

In most cases of previous approaches, the optical waves can only be dynamically manipulated in 1D. For example, Lim et al. utilized germanium-based metasurfaces to realize the ultrafast modulation of the transmission amplitude of the THz waves (**Figure 6**a,b).[167] The proposed metasurface is composed of periodic asymmetric split ring resonators which are fully embedded in a germanium thin film, as shown in Figure 6a. The dynamic manipulation of THz transmission amplitude is attributed to the excitation of the free carriers in germanium film by adding a pump beam. The modulation depth of the

THz transmission amplitude in the proposed design achieved 90% with a full recovery time equal to 17 ps. Electrically controlling and thermal controlling are also effective approaches for the realization of dynamic amplitude manipulation of optical waves by utilizing 2D materials and phase change materials.[60,168,169] For example, Ou et al. proposed a thermally reconfigurable metasurface to realize a reversible modulation of transmission amplitude of optical waves with modulation depth up to 50%.[168] For the implementation of the dynamic phase manipulation of optical waves, phase change materials are always utilized.[170,171] Chu et al. proposed a dielectric metasurface composed $Ge_2Sb_2Te_5$ (GST) nanorods to realize the independent phase modulation of optical waves in subwavelength scale (Figure 6c,d).[171] The optical response of the GST nanorods can be easily tuned by changing the phase state of GST between the crystalline state and the amorphous state. Thus, each single GST nanorod has two different delay effects on the phase of the optical waves. By changing the phase state of the GST nanorod independently, different phase profiles can be realized along the metasurfaces, as shown in Figure 6d. The proposed GST-based metasurfaces provide an alternative way for the wavefront modulation of optical waves. With the effective phase manipulation of optical waves, the polarization state of optical waves can also be dynamically manipulated.[129,132,172] Li et al. proposed graphene-loaded metasurfaces to realize the continuous controlling of the polarization state of the reflected waves (Figure 6e–g).[129] As shown in Figure 6e, the proposed hybrid metasurface consists of a graphene layer and periodic gold rectangular apertures. The polarization-selective near-field enhancement induced by the anisotropic optical response of the rectangular apertures will significantly enhance the interaction between incident waves and the graphene layer in y direction. Thus, the phase of y-component of the reflected waves can be continuous controlled with graphene layer by applying different gate voltages. With continuous manipulation of phase of reflected waves in y direction, the phase delay between x and y directions can be accordingly modulated, which results in the continuous manipulation of the polarization state of reflected waves, as shown in Figure 6f,g. Instead of involving reconfigurable materials or elastic substrates, the dynamic frequency manipulation of optical waves is achieved recently by mechanical approaches.[173–175] Li et al. demonstrated the rotational Doppler effect in linear and nonlinear optics by using half-wave plates or nonlinear crystals driven by separated motors, and showed the correlation between the rotational symmetry of the crystal and the nonlinear Doppler frequency shift (Figure 6h,i).[173] The results show that in linear optics, when the rotational angular frequency of the half-wave plate is equal to Ω, the transmitted circularly polarized wave with the opposite sense will have a frequency shift of $\pm 2\Omega$ compared to the normal circularly polarized incident waves. In addition, in nonlinear optics, when the rotational angular frequency of a nonlinear crystal with C3 rotationally symmetric is equal to Ω, the transmitted circularly polarized second harmonic wave with the opposite sense will have a frequency shift of $\pm 3\Omega$ compared to the normal circularly polarized fundamental incident waves. The proposed Doppler effect has been widely used in the design of both linear and nonlinear metasurfaces to realize novel optical functionalities and phenomenon.[174,175]
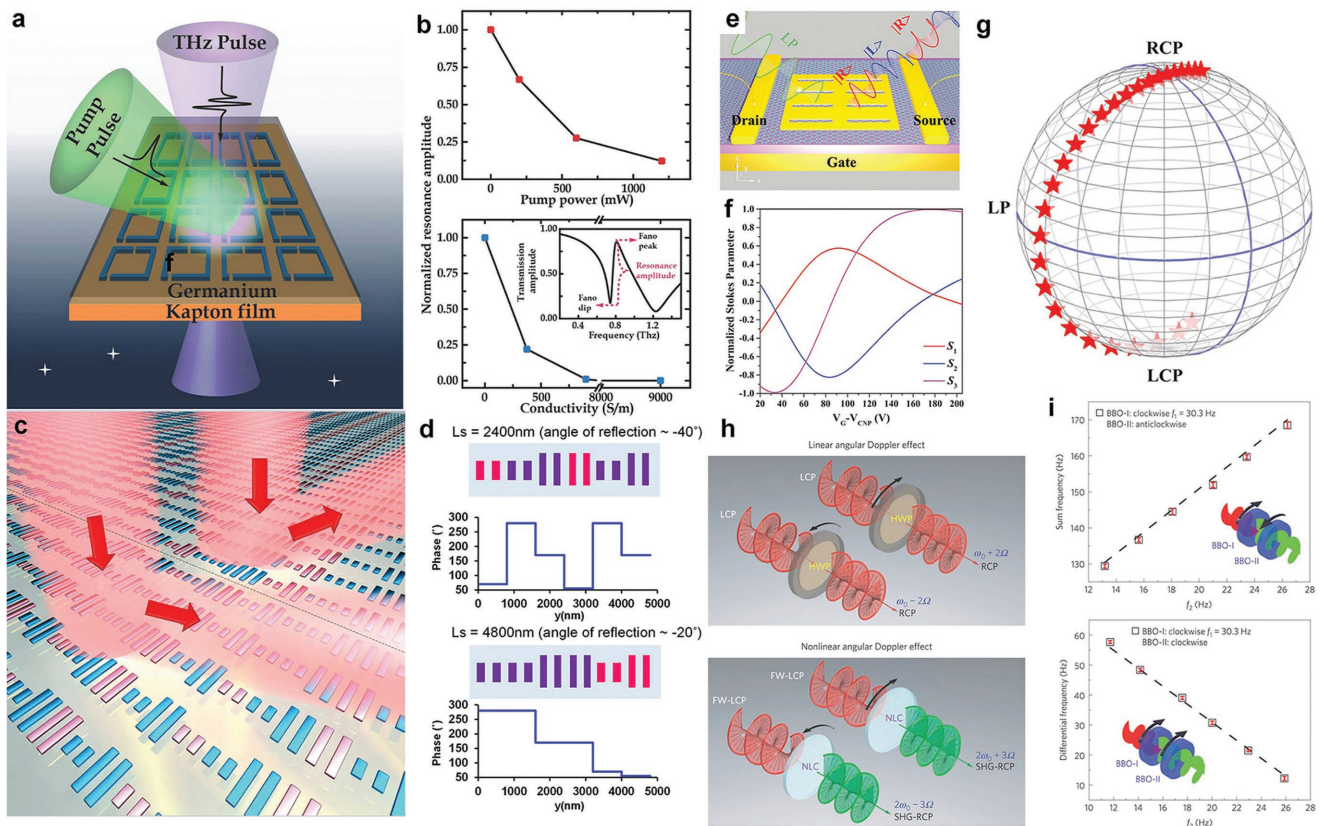
Figure 6. a) Artistic rendering of a germanium-based metasurface for ultrafast all-optical switching in THz regime. b) Experimental (top half) and simulated (bottom half) results of normalized resonance amplitude (difference between transmission levels at the THz dip and the THz peak) under different optical pump power at a pulse delay time of 4.7 ps. c) Artistic rendering of a tunable gradient metasurface composed of GST nanorods. d) The working principle of the GST-based tunable gradient metasurface. The pink GST nanorods are in crystalline phase and the purple GST nanorods are in amorphous phase. e) Schematic of the graphene-loaded metasurface for optical polarization encoding. f) The variation of stokes parameters with gate voltage. g) The variation of polarization state of reflected waves on the Poincare sphere under different gate voltage. h) Schematic of the optical linear and nonlinear rotational Doppler effect. i) Rotational Doppler shift of the second harmonic waves. a,b) Reproduced with permission.[167] Copyright 2018, Wiley-VCH. c,d) Reproduced with permission.[171] Copyright 2016, Wiley-VCH. e–g) Reproduced with permission.[129] Copyright 2015, Wiley-VCH. h,i) Reproduced with permission.[173] Copyright 2016, Nature Publishing Group.

In the past few years, researchers have made massive efforts on the implementation of dynamic manipulation of optical waves in 1D. Nowadays, even there are many approaches to realize the dynamic manipulation of amplitude, phase, polarization, and frequency of optical waves, there is still a long way to go. Further researches on reconfigurable metasurfaces with compact designs, high modulation depth, and ultrafast response time are still needed. Especially, realizing fully dynamic phase controlling of optical waves in subwavelength scale is yet to be experimentally presented. Moreover, researches of realizing the independent dynamic manipulation of optical waves in multidimensions are still a blank.

3. 2D Manipulation of Optical Waves with Metasurfaces

The recent approaches we discussed in Section 2 typically focus on single-dimensional manipulation of optical waves and the realization of single optical functionalities, which are quite not enough for the acquisition of any optical devices on demand.

Nowadays, researchers in this area focus on the improvement of the performance (efficiency, bandwidth, achromatism, and so on) of the optical devices based on metasurfaces and the achievement of integrated multifunctional optical devices by skillfully utilizing multidimensional manipulation of optical waves with metasurfaces. In this section, recent works related to 2D manipulation of optical waves with metasurface are discussed typically, which is the hot spot in related research area of metasurfaces.

3.1. Manipulating Amplitude and Phase of Optical Waves Simultaneously

The transmission of complete imaging information in scalar optics requires both amplitude and phase modulations, as the wave equation $|\Psi\rangle = Ae^{-i\phi}$ implies. However, conventional imaging or holography techniques are usually limited by the amplitude- or phase-only modulation schemes, which is not the full information of object images.[176–180] Independently simultaneous control of amplitude and phase with metasurfaces
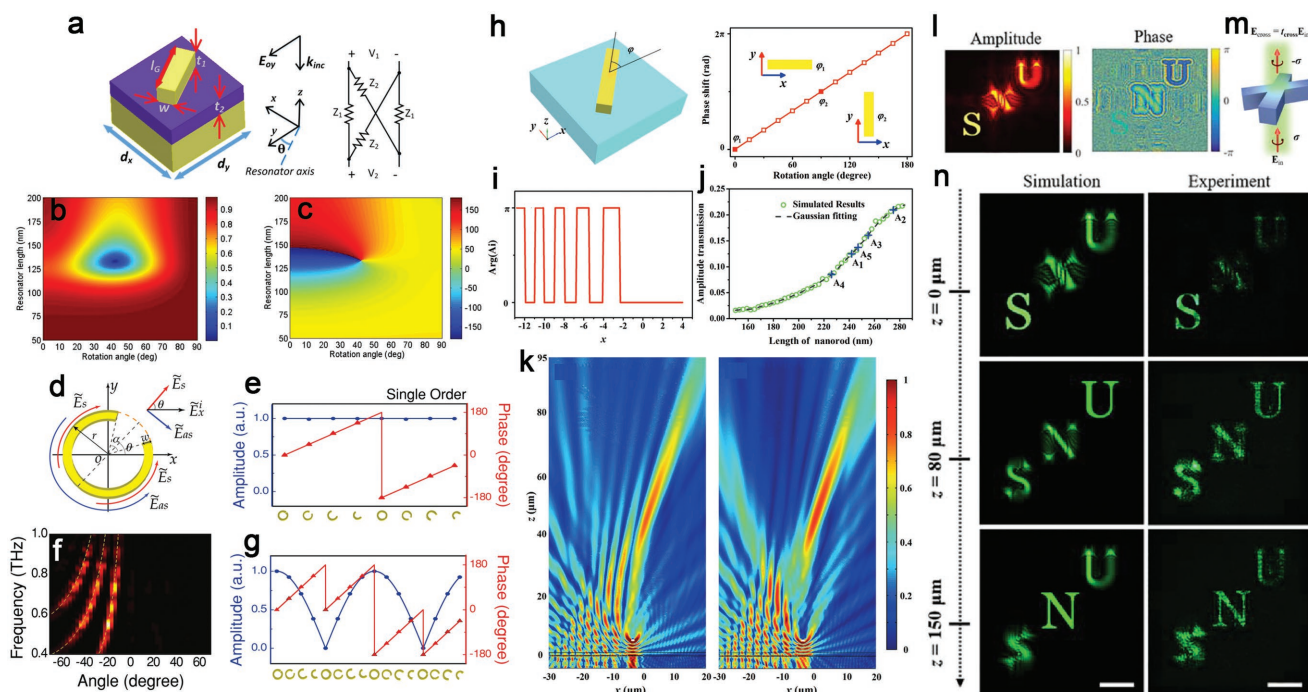
Figure 7. a) The schematic of a nanorod gap-surface plasmon resonator that forms the Huygens' metasurfaces. The equivalent circuit model depicts that orthogonal electric and magnetic responses can be simultaneously achieved, which is essential to control an optical surface's local reflection coefficients. b,c) Variation in amplitude (b) and phase (c) of the reflection coefficients for different resonator lengths and rotation angles. This result shows the resonator is capable of manipulating amplitude and phase. d) Schematic of C-shaped antenna. This antenna supports symmetric mode E_s and antisymmetric mode E_{as}. With different geometric parameters the C-shaped antenna scatters the incident light with different strength and phase. e) Simulated amplitude and phase profiles along the x-axis for a sample with a single diffraction order. f) Measured diffraction intensity for a sample with first, second, and third order. g) Simulated amplitude and phase profiles along x-axis for a sample of first and third diffraction order at 0.63 THz. h) A unit cell with a gold nanorod can completely control phase of the scattered light utilizing the Pancharatnam–Berry phase. i) Phase pattern of the Airy function using discrete algorithm. j) The amplitude of the scattered light can be controlled by choosing different lengths of the nanorods. k) Simulated electric distributions of the Airy beam, with a rectangular scatterer of the size 1 μm × 0.5 μm located at x = −3 μm and z = 5 μm. l) Computed amplitude and phase distribution of the computer generated hologram with 600 × 600 pixels. m) Schematic of the X-shaped unit cell that can manipulate amplitude and phase of the incident light. n) Simulated and measured intensity distribution shows the amplitude–phase combined method suppresses significant noises, advancing the quality of holographic images in 3D space. a–c) Reproduced with permission.[185] Copyright 2014, American Physical Society. d–g) Reproduced with permission.[187] Copyright 2014, Wiley-VCH. h–k) Reproduced with permission.[188] Copyright 2016, Wiley-VCH. l–n) Reproduced with permission.[189] Copyright 2017, Royal Society of Chemistry.

requires more degree of freedom to manipulate the optical field, without introducing unpractical nanostructures.[181–184] Kim et al. proposed a nanorod gap-surface plasmon resonator to form Huygens' metasurfaces in the optical waveband (**Figure 7**a).[185] This resonator can simultaneously stimulate electric and magnetic dipoles, which enables the Huygens' antenna capable of manipulating the complex reflection and minimizing the excitation of unwanted plane waves. With varied resonator lengths and rotation angles, the amplitude and phase of the scattered light can be efficiently modulated (Figure 7b,c). The efficiency of the resonators reaches 40% for an operating wavelength of 800 nm. Another effective method to simultaneously control amplitude and phase is utilizing C-shaped antennas.[186,187] This antenna supports both symmetric and antisymmetric current modes, just as the V-shaped antenna does as mentioned previously. The generated scattered electric E_y can be written as $E_y = 0.5E_x \sin(2\theta)(A_s e^{i\phi_s} + A_{as} e^{i\phi_{as}})$, where A_s, A_{as}, and ϕ_s, ϕ_{as} denote the strength and phase of the symmetric and antisymmetric modes, θ is the orientation angle of the antenna (Figure 7d). The amplitude varies

as $|\sin(2\theta)|$, which can be controlled independently of the phase factor of E_y. Diffractive devices have been designed to demonstrate the ability of simultaneous manipulation of amplitude and phase (Figure 7e–g).[187] Although the metasurface is designed working at 0.63 THz, the device persists its functionality over a broadband range from 0.5 to 1.0 THz. Similarly, nanorod can also manipulate amplitude and phase with varied geometric parameters and orientation angles, as shown in Figure 7h. As the nanorod rotates, the phase of the scattered light linearly increases due to Pancharatnam–Berry phase accumulation. Li et al. utilized this nanorod antenna to realize Airy phase distribution (Figure 7i).[188] Interestingly, the intensity of the scattered light depends on the length of the nanorods (Figure 7j), which means the amplitude and phase can be independently controlled by choosing different length and orientation of antennas. When a rectangular scatterer is put in the optical field, it can be seen that the generated Airy beam heals itself after passing the scatterer as expected. With the lack of amplitude modulation, the Airy beam is in chaos when passing the block, while with simplified amplitude modulation the Airy

beam heals itself when passing the block (Figure 7k). However, the efficiency of such nanorod resonators or split ring resonators is limited below 25%, since the generated electric or magnetic dipoles radiate to two opposite directions, and the incident light is partially converted to the signal polarization.[186]

The abovementioned methods for simultaneous control of amplitude and phase suffer from low efficiency, which can be improved by dielectric metasurfaces. Lee et al. proposed a broadband holographic metasurface comprising X-shaped polycrystalline silicon unit cells (Figure 7l–n) that can convert circularly polarized light into the cross-polarized component. By designing complex-amplitude holograms, amplitude and phase profiles of the computer-generated holograms have been illustrated. It can been seen that the holography remains of high quality in the 3D space without speckle noises in a typical phase-only hologram.[189] Moreover, the proposed metasurface is a broadband one, which can be attributed to two aspects: 1) All-dielectric metasurfaces are based on Mie scattering, which can be easier designed with less sensitivity in the frequency domain compared with plasmonic building blocks. 2) The optical manipulation of the unit cell originates from the geometric phase, a topological characteristic depending only on the orientation of the structure. Recently, the challenge for simultaneous control of amplitude and phase mainly lies in considering other optical dimensions, such as achieving such control in an ultrafast time scale or for anisotropic incident polarizations. The manipulation of both amplitude and phase may expand the superior limitation of various photonic applications, such as 3D biological imaging, optical computing.

3.2. Manipulating Phase and Polarization of Optical Waves Simultaneously

In vectorial optics, many intriguing phenomena occur, which seem impossible in scalar optics. For example, vector beams can be utilized to achieve longitudinally polarized light and sub-diffraction focusing spot.[190–192] Recently, simultaneous control of polarization and phase has been extensively investigated. Li et al. proposed bilayer plasmonic metasurfaces that can manipulate phase by adjusting the relative position of the two layers, and manipulate polarization by varying the orientation of the unit cells in the near infrared waveband (**Figure 8**a,b).[193] The simultaneous control of transmitted phase and polarization can be realized, as shown in Figure 8c. With given phase shift and polarization, the geometry of the doublet metasurface can be obtained. The measured light intensity with an analyzer in front of the charge coupled device (CCD) camera shows that the transmitted light is a radially polarized beam. Arbitrary spatial variation of phase and polarization can also be achieved by such metasurfaces,[194] with any required polarization distribution and topological charges of efficiency about 16%. Mueller et al. combined geometric and propagation phases, which realized arbitrary phase abrupt on any two predefined orthogonal polarization states.[195] The building blocks of the metasurface are silicon nanoblocks and can be designed approaching unitary efficiency. The geometric size determines the propagation phase, and the orientation of the nanoblocks determines the geometric phase. With different circularly polarized incidence, the holograms exhibit completely different images (Figure 8d,e). This strategy enlarges the design space for polarization-sensitive metasurface-based imaging and holography devices.

Recently, the complete control of polarization and phase with unitary efficiency is achieved through elliptical nanopillars working at 915 nm incidence.[196] Since each pixel of the metasurface can be designed to realize any symmetric and unitary Jones matrix, the transmission matrix of the nanopillars enables full control of polarization and phase. As shown in Figure 8f, an RCP incident light is focused to a spot, while an LCP light is focused into a doughnut-shaped small region. This platform also provides independent and complete phase modulation for two orthogonal polarization states, and further applications such as integrated conformal optical devices can be expected. Recently, the arbitrary spin-to-orbital angular momentum conversion has drawn much attention of the scientific community, which has profound applications in quantum optics.[197–202] Devlin et al. proposed a method using high-index dielectric metasurfaces to efficiently convert spin angular momentum to orbital angular momentum. Arbitrary values of orbital angular momentum can be achieved under circularly polarized incidence, and the device output along a predefined path on the higher order Poincaré sphere is investigated. As shown in Figure 8g, a generalized spin-to-orbit conversion is also realized. Another way to achieve control of phase and polarization is utilizing cascaded metasurface (Figure 8h). This metasurface consists of four anisotropic sheet admittances, each of which can be modeled as a parallel inductive–capacitor circuit (LC circuit). The color in Figure 8h represents the average transmittance for the two polarizations, and the blue box indicates the region with full control of the transmitted phase for both polarization states. Li et al. proposed C3 symmetric nonlinear metasurface for spin-to-orbital angular momentum conversion in SHG.[204] As shown in Figure 8i,j, the incident LCP light is converted to RCP second harmonic one (without generation of LCP light due to selection rules[203,204]). The topological charges are measured using linearly polarized incidence to get a self-interference of the vortex beam.

3.3. Manipulating Amplitude and Frequency of Optical Waves Simultaneously

For linear optical response, simultaneous manipulation of amplitude and frequency of optical waves with metasurfaces will lead to important real applications. The unique frequency-dependent absorption and scattering properties of metasurfaces in the visible region are utilized to print color at the nanoscale, which is known as structural colors. Compared to traditional pigments, metasurfaces provide high spatial resolution, durable and single material colors, which show a profound commercial value in high-resolution color printing, imaging, biosensing, and so on.[29,205] Plasmonic metasurfaces with gold, silver, or aluminum nanostructures have been widely used for the realization of structure colors.[206–210] However, the absorption losses, low resonance quality factors, prohibitive cost, and limited stability of plasmonics metasurfaces prevent them to the generation of structural colors with high color purity. Recently,
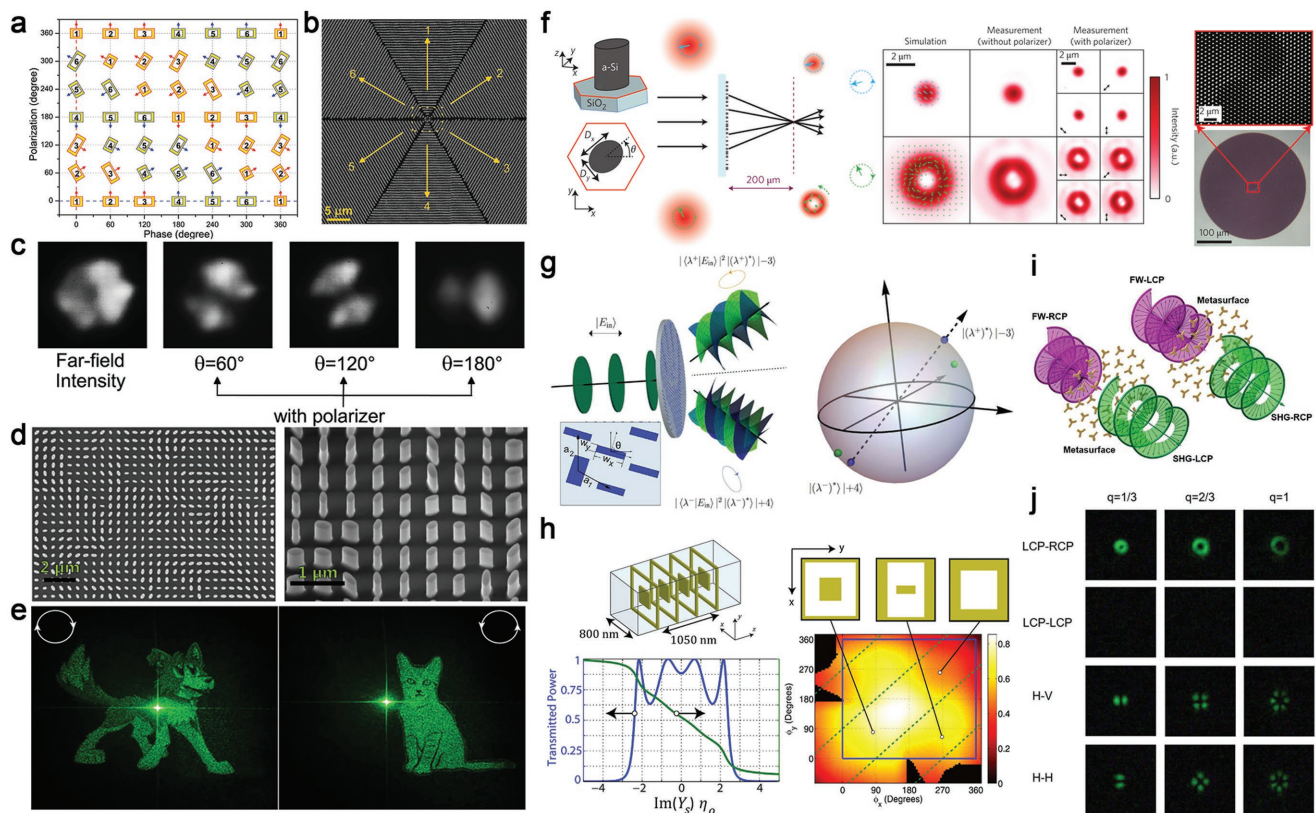
Figure 8. a) Nanoaperture pairs with various geometries and orientations to realize metasurfaces for the complete control of the transmitted polarization and phase. b) SEM image of the sample designed to generate radially polarized vector beam. The sample is composed of six different areas corresponding six linear polarization. c) Measured far-field intensity distribution of the generated radially polarized beam, with and without a polarization analyzer in front of the CCD camera. d) SEM image of the dielectric metasurface encoding the holograms with 350×350 μm^2 in size and contains 420 000 TiO$_2$ nanopillars. e) With illumination of RCP/LCP, the metasurface produces an image of a cartoon dog/cat to the far field. The bright dot in the middle of each image is due to the zero-order light not coupling into the metasurface. f) Full control of polarization and phase with silicon nanopillars. Different circularly polarized incident light is focused to a single spot or a doughnut-shaped spot. g) Schematic of the dielectric device that maps elliptically polarized incidence to two independent states of orbital angular momentum. Inset: the building block the spin-to-orbital angular momentum conversion. h) Schematic view of a typical unit cell with four layers of subwavelength structures. The transmitted power and phase alter as a function of the normalized sheet admittance. The intensity map represents the average transmittance for the two polarizations. i) Schematic of the spin controlled generation of orbital angular momentum of second harmonic signal by using C3 symmetric nonlinear metasurfaces. j) Measured intensity of second harmonic signal with $q = 1/3$, 2/3, and 1. Circularly polarized incidence to demonstrate the spin-to-orbital angular momentum conversion, and linearly polarized incidence to identify the topological charge. a–c) Reproduced with permission.[193] Copyright 2015, Wiley-VCH. d,e) Reproduced with permission.[195] Copyright 2017, American Physical Society. f) Reproduced with permission.[196] Copyright 2015, Nature Publishing Group. g) Reproduced with permission.[201] Copyright 2017, American Association for the Advancement of Science. h) Reproduced with permission.[202] Copyright 2013, American Institute of Physics. i,j) Reproduced with permission.[204] Copyright 2017, American Chemical Society.

dielectric metasurfaces are utilized to generate distinct structural colors effectively with low absorption losses.[211–215] Flauraud et al. utilized silicon nanodiscs to realize nanoscale color reproduction with a broad coverage and vivid color palette (**Figure 9**a,b).[215] They compared the optical spectrum of silicon nanodiscs with those of silver and aluminum nanostructures in various geometric and illumination conditions, and the results show that the silicon nanodisc arrays are optimized for the realization of millimetric paining replicas as well as high resolution color features. This work shows tremendous application potential of Si-based structural colors in nanoscale color elements. Compared with polarization-independent structural colors, color filters or polarization-dependent structural colors based on metasurfaces have also been widely investigated for its potential applications in polarization imaging, active color

pixels, and so on.[216–220] Duempelmann et al. utilized silver nanowires to realize a fourfold plasmonic color filter, the output color can be changed by simply rotating a polarizer (Figure 9c–e).[219] Polarization sensitive structural colors have also been proposed in dielectric metasurfaces. Wiecha et al. realized colour pixels generation based on silicon building blocks, which has resonant modes at two optimized and polarization-dependent wavelengths by employing evolutionary multiobjective algorithms.[220]

For nonlinear optical response, simultaneous manipulation of amplitude and frequency of optical waves with metasurfaces is beginning to show some important applications in sensing, imaging, and anticounterfeiting.[221–223] Rodrigues et al. investigated the chiral-selective nonlinear optical response of twisted-arc nanostructures and realized high-contrast second

**ADVANCED
SCIENCE NEWS**

www.advancedsciencenews.com

**ADVANCED
MATERIALS**

www.advmat.de
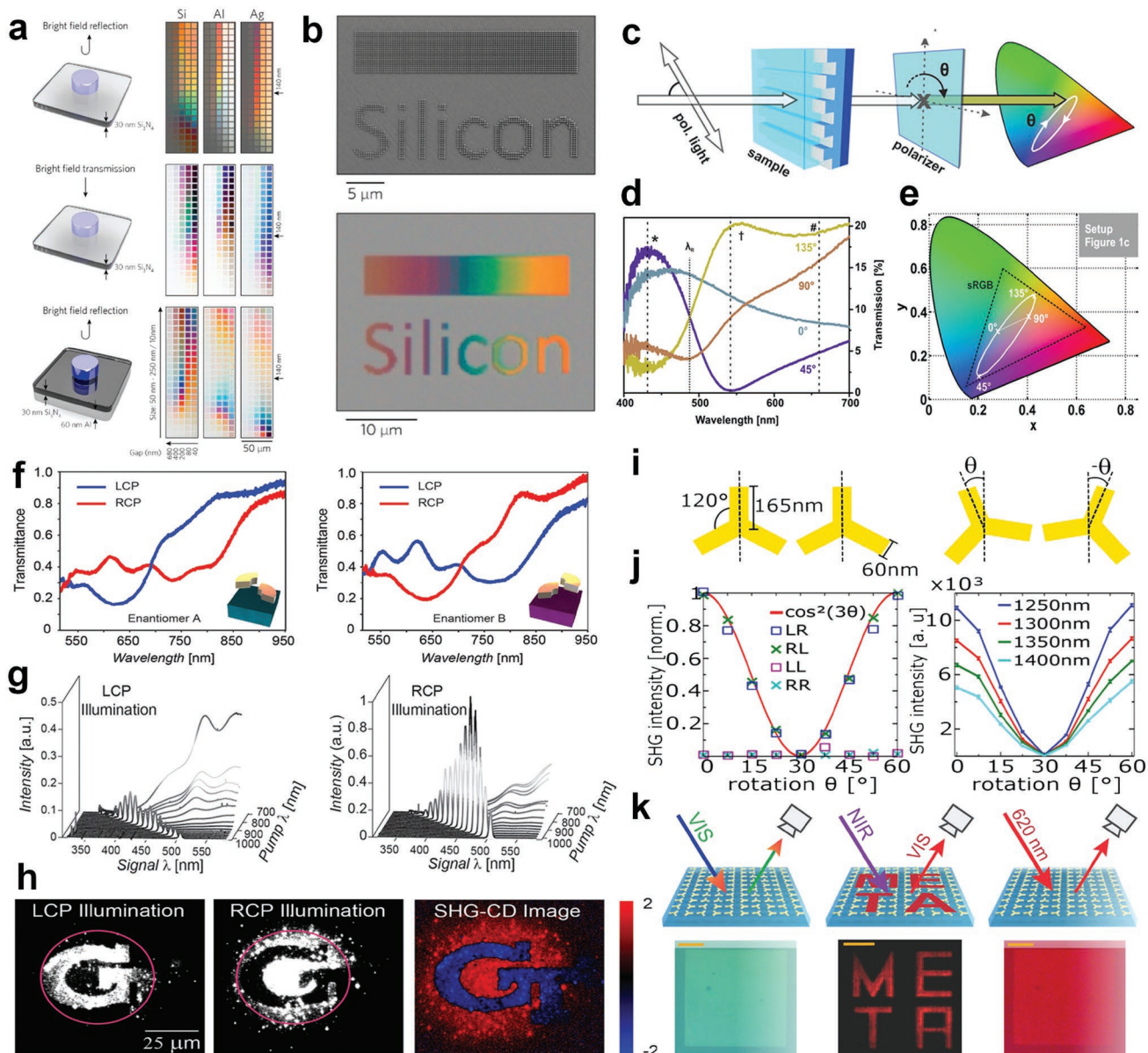
Figure 9. a) Bright field measurements for Si, Al, and Ag nanodisks. b) SEM and optical microscopy image of a gradient array and the word "Silicon" composed of Si nanodisks. c) Schematic of the designed fourfold color filter. d) The experimental measured transmission spectra of the color filter with a variable analyzing polarizer. e) CIE xyY color plot of the measured transmission spectrum in (d). f) Measured transmission spectrum of two unit cells of the chiral metasurface for circularly polarized light. g) Nonlinear signals of enantiomer A excited by LCP and RCP pump light. h) Two nonlinear images of the "GT" patterned logo and the SHG-CD. The inner and the outer regions of the logo host the B and A enantiomers, respectively. i) Schematic of the unit cell of the nonlinear metasurface. j) (Left plane) Angle-dependent SHG intensity for different fundamental wave polarizations. (Right plane) Measured RCP SHG intensity for different orientation angle θ of meta-atoms for LCP fundamental waves. k) Working principle of the nonlinear metasurface for different illumination conditions and the corresponding measured real space microscopy images. a,b) Reproduced with permission.[215] Copyright 2017, American Chemical Society. c–e) Reproduced with permission.[219] Copyright 2016, American Chemical Society. f–h) Reproduced with permission.[222] Copyright 2014, Wiley-VCH. i–k) Reproduced with permission.[223] Copyright 2017, American Chemical Society.

harmonic optical imaging (Figure 9f–h).[222] This work provides a prospect of the nonlinear chiral metasurfaces, and serves as an alternative way for the study of chirality sensitive materials. Walter et al. utilized nonlinear metasurface to realize optical image encoding (Figure 9i–k).[223] The encoded image can only be obtained by collecting the SHG signals of the metasurfaces. This novel phenomenon is attributed to the effective modulation of the

interferences of SHG waves between neighboring meta-atoms. By manipulating the orientation angles of two neighboring meta-atoms, local SHG intensity can be continuously tailored (Figure 9j). This work provides valuable insight for anticounterfeiting with metasurfaces. The simultaneous manipulation of amplitude and frequency of optical waves based on metasurfaces has remarkable impact in the areas of imaging and anticounterfeiting.

**ADVANCED
SCIENCE NEWS**

www.advancedsciencenews.com

**ADVANCED
MATERIALS**

www.advmat.de

3.4. Manipulating Phase and Frequency of Optical Waves Simultaneously

Besides utilizing metasurface to enhance the nonlinear optical response, metasurfaces with efficient phase modulation of nonlinear waves have received great attention in recent years for their great value in the realization of many novel nonlinear functionalities.[22,27,36] Current researches indicated that metasurfaces provide a direct and an effective way for nonlinear phase manipulation.[224–226] Li et al. provided an effective way for continuous manipulation of phase of harmonic waves with nonlinear metasurfaces (**Figure 10**a).[224] For fundamental beams with circular polarization, the phase of the nonlinear polarization of the artificial structure can be effectively tuned by varying the orientation angles of the structure. For structures with orientation angle of θ, the results show that the phase of the nonlinear polarizabilities of the nth harmonic generation is $(n - 1)\sigma\theta$ and $(n + 1)\sigma\theta$, for the same and the opposite polarization to that of the fundamental wave, respectively. This continuous phase manipulation provides an alternative way for simultaneous manipulation of phase and frequency of optical waves with metasurface. Effective approaches for nonlinear phase manipulation with linearly polarized fundamental beams have also been proposed. Segal et al. utilized split-ring resonators (SRRs) to demonstrate unprecedented manipulation over the nonlinear emission with linearly polarized fundamental beams (Figure 10b,d).[225] A mirror inversion of the SRR with respect to its base will have a minimal effect on the fundamental beam but will induce π phase shifts on the second harmonic currents and the locally generated second harmonic

radiation. With this approach, engineered nonlinear diffraction, ultrawide all-optical scanning, and intense focusing of the nonlinear signal have been well demonstrated. Almeida et al. further demonstrated full nonlinear phase manipulation from 0 to 2π for four-wave mixing with linear polarized fundamental beams.[226] This full phase manipulation is attributed to a spatially varying phase response of a metallic metasurface whose unit cell designed specifically for the frequency of the nonlinear signal. Compared with the proposed method in Figure 10a, this method may have some complexity on structure design since the nonlinear responses in metasurfaces are quite sensitive to the variations of the structure parameters.

With the rapid development of this research field, metasurfaces with simultaneous efficient nonlinear response and sub-wavelength phase control have also been proposed.[227,228] By combining the metasurfaces and the semiconductor multiquantum wells, Nookala et al. experimentally demonstrated continuous beam steering of the giant nonlinear second harmonic (Figure 10e,f).[228] This result indicates that full manipulation of the phase of the nonlinear signal can be achieved at the individual nanoresonator level, which allows us to realize arbitrary manipulation of the wavefront of SHG signals with sub-wavelength resolution. Moreover, based on the simultaneous manipulation of phase and frequency of optical waves with metasurfaces, numerous novel nonlinear functionalities have also been realized.[229–232] One key application is the nonlinear holograms. Ye et al. experimentally demonstrated a polarization and wavelength multiplexed nonlinear metasurface holography. For optical waves with different frequency/polarization combinations, independent holographic images
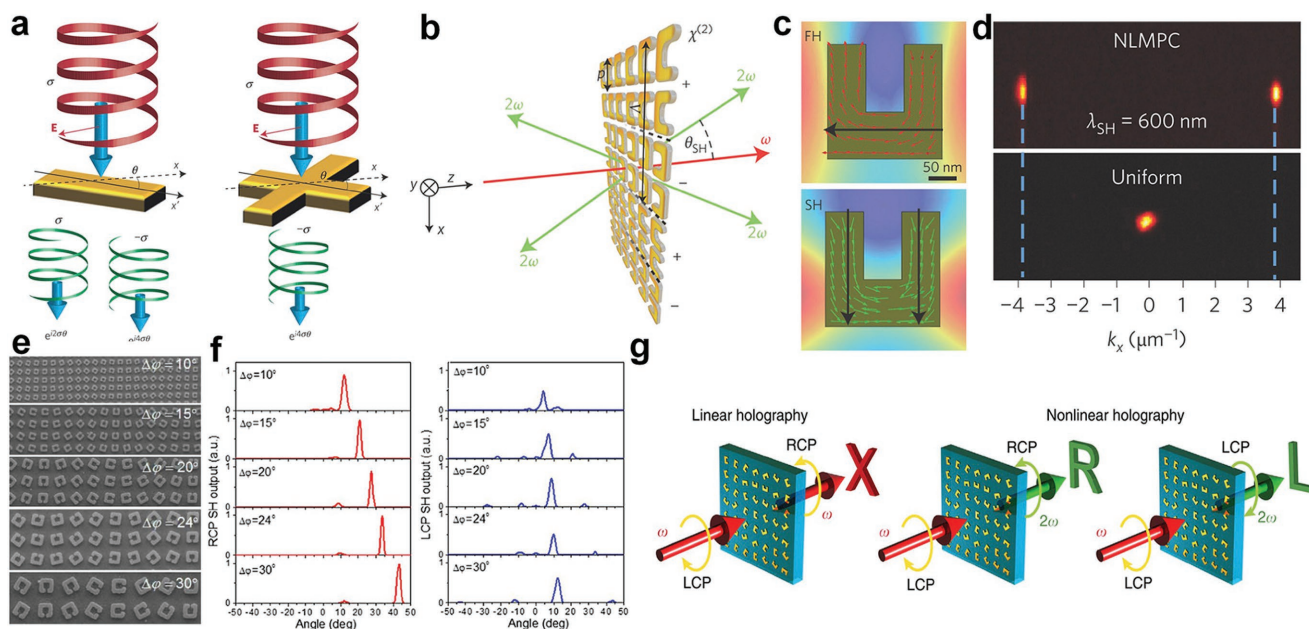
Figure 10. a) Illustration of geometric-phase-controlled nonlinear metasurface. b) Illustration of a nonlinear metasurface with 1D modulation of $\chi^{(2)}$. c) Calculated fundamental harmonic surface currents and generated second harmonic currents. d) k-space images of emitted forward second harmonic from the designed nonlinear metasurface. e) SEM of phase gradient nonlinear metasurfaces, with differing angular rotational steps. f) Far field profiles of RCP and LCP second harmonics. g) Linear and second harmonic generation holographic images in a nonlinear hologram metasurface. a) Reproduced with permission.[224] Copyright 2015, Nature Publishing Group. b–d) Reproduced with permission.[225] Copyright 2015, Nature Publishing Group. e,f) Reproduced with permission.[228] Copyright 2016, Optical Society of America. g) Reproduced with permission.[232] Copyright 2016, Nature Publishing Group.

can be constructed at the same spatial area (Figure 10g).[232] This work indicates that multiplexed nonlinear metasurface holography provides an alternative way for optical anticounterfeiting and encryption. Realizing effective phase manipulation of nonlinear optical waves with giant nonlinear response in metasurfaces will greatly expand the applications of metasurfaces in nonlinear optics and optical encryption.

4. Conclusions and Outlook

Herein, we regarded the optical parameters as different dimensions that determine the functionalities of an optical device. We reviewed metasurfaces for single-dimensional manipulation of optical waves, such as amplitude, phase, polarization, and frequency. We also reviewed the applications based on 2D manipulation of optical waves. With high abilities of increasing the light–matter interaction, metasurfaces provide a distinguished platform to produce novel phenomena that cannot be found in conventional optical media. However, the manipulation of optical field in single dimension restricts the expansion of high performance devices, such as super resolution with vector beams, which requires simultaneous control of phase and polarization.[190] Recently, the multidimensional manipulation of optical waves by metasurfaces arises, which opens up the possibility of parallel and independent control of different dimensions of optical fields. We reviewed the independent manipulation of amplitude–phase, phase–polarization, amplitude–frequency, phase–frequency, and the corresponding applications. This revolutionary capability of simultaneous control of multiple dimensions of optical field enabled by metasurfaces makes it possible to produce more novel phenomena, and to encourage more available applications, such as the accurate and robust transmission of optical information. One significant advantage of multidimensional manipulation is to realize integrated photonic devices,[233–235] which may strikingly reduce the size and enhance the performance of the devices due to the compact manipulation. Another intriguing application is artificial intelligence enhanced photonic techniques, such as a photonic neural network. By exploiting machine-learning techniques, the photonic system design will be much efficient and optimized.[236,237] Similar operations can also be applied in photonic hardware design, data processing, and analysis. We believe that future metasurfaces with optical dimensional manipulation will greatly advance the realization of optical computation, biological sensing, and so on, and will promote the life-style in our daily life.

We envision several promising directions in multidimensional manipulation of optical waves which may have profound impact on photonic nanosystems.

Development of New Optical Dimensions: The optical parameters are not limited to the abovementioned ones. The recent burgeoning topological metasurfaces provide another optical dimension, which take advantage of topology to realize robust optical transmission, and other novel phenomena in energy band.[238,239] Moreover, instantaneous, ultrafast, and active manipulation of optical field in nanosecond or femtosecond is another dimension that characterizes time evolution instead of the steady states to explore the light–matter interaction.[240] Due to the development of nanofabrication techniques, quantum entanglement realized by metasurfaces has drawn much attention of researchers,[241] which may greatly boost the exploitation of the quantum photonics. With the increase of optical manipulation dimensions, the development of manipulating optical parameters with metasurfaces may profoundly affect the nanophotonic exploitation nowadays.

Arbitrary Dimensional Manipulation of Optical Waves: As discussed herein, the current optical field manipulation is mainly single-dimensional and 2D manipulation. It is challenging to realize independent manipulation of three or arbitrary dimensions of optical waves, since the optical dimensions are basically associated with each other when varying the geometrical parameters of the meta-atoms. One way to realize arbitrary dimensional manipulation of optical waves is to find a space or a method to attribute each optical dimension to different mathematical part, and to find the relationship between meta-atoms and each dimensional term, which may phenomenologically simplify the realization of arbitrary control of optical fields. If the manipulation of optical waves in arbitrary dimension can be achieved, the optical devices can be designed on demand.

Integrated Optical Dimensional Manipulation: An emerging theme in metasurfaces research is to realize integrated optical manipulation. The anisotropic, dispersive, and coupling properties of subwavelength nanostructures provide versatile and unprecedented possibilities of optical manipulation in almost all wavelength ranges. The planar platform of metasurfaces, especially all-dielectric metasurfaces, is compatible with industrialized CMOS techniques. With the development of novel design principles,[242,243] fabrication technologies, planar waveguide, and sensing architectures,[244,245] integrated and on-chip optical dimensional manipulation techniques are more and more feasible nowadays.

Conflict of Interest

The authors declare no conflict of interest.

[1] N. I. Zheludev, *Science* **2010**, *328*, 582.
[2] Y. Liu, X. Zhang, *Chem. Soc. Rev.* **2011**, *40*, 2494.
[3] N. I. Zheludev, *Science* **2015**, *348*, 973.

[4] D. R. Smith, W. J. Padilla, D. C. Vier, S. C. Nemat-Nasser, S. Schultz, *Phys. Rev. Lett.* **2000**, *84*, 4184.

[5] R. Shelby, D. Smith, S. Schultz, *Science* **2001**, *292*, 77.

[6] S. Zhang, W. Fan, N. C. Panoiu, K. J. Malloy, R. M. Osgood, S. R. J. Brueck, *Phys. Rev. Lett.* **2005**, *95*, 137404.

[7] D. Schurig, J. J. Mock, B. J. Justice, S. A. Cummer, J. B. Pendry, A. F. Starr, D. R. Smith, *Science* **2006**, *314*, 977.

[8] W. Cai, U. K. Chettiar, A. V. Kildishev, V. M. Shalaev, *Nat. Photonics* **2007**, *1*, 224.

[9] D. A. Genov, S. Zhang, X. Zhang, *Nat. Phys.* **2009**, *5*, 687.

[10] A. V. Rogacheva, V. A. Fedotov, A. S. Schwanecke, N. I. Zheludev, *Phys. Rev. Lett.* **2006**, *97*, 177401.

[11] J. K. Gansel, M. Thiel, M. S. Rill, M. Decker, K. Bade, V. Saile, V. F. Georg, S. Stefan, M. Wegener, *Science* **2009**, *325*, 1513.

[12] N. I. Zheludev, Y. S. Kivshar, *Nat. Mater.* **2012**, *11*, 917.

[13] A. V. Kildishev, A. Boltasseva, V. M. Shalaev, *Science* **2013**, *339*, 1232009.

[14] N. Meinzer, W. L. Barnes, I. R. Hooper, *Nat. Photonics* **2014**, *8*, 889.

[15] H. H. Hsiao, C. H. Chu, D. P. Tsai, *Small Methods* **2017**, *1*, 1600064.

[16] M. Kauranen, A. V. Zayats, *Nat. Photonics* **2012**, *6*, 737.

[17] A. Poddubny, I. Iorsh, P. Belov, Y. Kivshar, *Nat. Photonics* **2013**, *7*, 948.

[18] N. Yu, F. Capasso, *Nat. Mater.* **2014**, *13*, 139.

[19] K. Y. Bliokh, F. J. Rodríguez-Fortuño, F. Nori, A. V. Zayats, *Nat. Photonics* **2015**, *9*, 796.

[20] H. Cheng, Z. Liu, S. Chen, J. Tian, *Adv. Mater.* **2015**, *27*, 5410.

[21] Y. Ra'Di, C. R. Simovski, S. A. Tretyakov, *Phys. Rev. Appl.* **2015**, *3*, 037001.

[22] H. T. Chen, A. J. Taylor, N. Yu, *Rep. Prog. Phys.* **2016**, *79*, 076401.

[23] A. M. Shaltout, N. Kinsey, J. Kim, R. Chandrasekar, J. C. Ndukaife, A. Boltasseva, V. M. Shalaev, *Proc. IEEE* **2016**, *104*, 2270.

[24] A. I. Kuznetsov, A. E. Miroshnichenko, M. L. Brongersma, Y. S. Kivshar, B. Luk'yanchuk, *Science* **2016**, *354*, aag2472.

[25] S. Jahani, Z. Jacob, *Nat. Nanotechnol.* **2016**, *11*, 23.

[26] N. I. Zheludev, E. Plum, *Nat. Nanotechnol.* **2016**, *11*, 16.

[27] A. E. Minovich, A. E. Miroshnichenko, A. Y. Bykov, T. V. Murzina, D. N. Neshev, Y. S. Kivshar, *Laser Photonics Rev.* **2015**, *9*, 195.

[28] A. M. Shaltout, A. V. Kildishev, V. M. Shalaev, *J. Opt. Soc. Am. B* **2016**, *33*, 501.

[29] A. Kristensen, J. K. Yang, S. I. Bozhevolnyi, S. Link, P. Nordlander, N. J. Halas, N. A. Mortensen, *Nat. Rev. Mater.* **2017**, *2*, 16088.

[30] N. M. Estakhri, A. Alù, *J. Opt. Soc. Am. B* **2016**, *33*, A21.

[31] Y. Xu, Y. Fu, H. Chen, *Nat. Rev. Mater.* **2016**, *1*, 16067.

[32] I. Staude, J. Schilling, *Nat. Photonics* **2017**, *11*, 274.

[33] W. Wan, J. Gao, X. Yang, *Adv. Opt. Mater.* **2017**, *5*, 1700541.

[34] F. Monticone, A. Alù, *Rep. Prog. Phys.* **2017**, *80*, 036401.

[35] P. Lalanne, P. Chavel, *Laser Photonics Rev.* **2017**, *11*, 1600295.

[36] G. Li, S. Zhang, T. Zentgraf, *Nat. Rev. Mater.* **2017**, *2*, 17010.

[37] X. Ling, X. Zhou, K. Huang, Y. Liu, C. W. Qiu, H. Luo, S. Wen, *Rep. Prog. Phys.* **2017**, *80*, 066401.

[38] A. Passaseo, M. Esposito, M. Cuscunà, V. Tasco, *Adv. Opt. Mater.* **2017**, *5*, 1601079.

[39] J. T. Collins, C. Kuppe, D. C. Hooper, C. Sibilia, M. Centini, V. K. Valev, *Adv. Opt. Mater.* **2017**, *5*, 1700182.

[40] L. Zhang, S. Mei, K. Huang, C. W. Qiu, *Adv. Opt. Mater.* **2016**, *4*, 818.

[41] N. I. Landy, S. Sajuyigbe, J. J. Mock, D. R. Smith, W. J. Padilla, *Phys. Rev. Lett.* **2008**, *100*, 207402.

[42] N. Liu, M. Mesch, T. Weiss, M. Hentschel, H. Giessen, *Nano Lett.* **2010**, *10*, 2342.

[43] H. T. Chen, *Opt. Express* **2012**, *20*, 7165.

[44] T. Cao, C. Wei, R. E. Simpson, L. Zhang, M. J. Cryan, *Opt. Mater. Express* **2013**, *3*, 1101.

[45] W. Zhou, K. Li, C. Song, P. Hao, M. Chi, M. Yu, Y. Wu, *Opt. Express* **2015**, *23*, A413.

[46] S. Chen, H. Cheng, H. Yang, J. Li, X. Duan, C. Gu, J. Tian, *Appl. Phys. Lett.* **2011**, *99*, 253104.

[47] H. Cheng, S. Chen, H. Yang, J. Li, X. An, C. Gu, J. Tian, *J. Opt.* **2012**, *14*, 085102.

[48] Z. Mao, S. Liu, B. Bian, B. Wang, B. Ma, L. Chen, J. Xu, *J. Appl. Phys.* **2014**, *115*, 204505.

[49] X. Duan, S. Chen, W. Liu, H. Cheng, Z. Li, J. Tian, *J. Opt.* **2014**, *16*, 125107.

[50] J. Zhu, Z. Ma, W. Sun, F. Ding, Q. He, L. Zhou, Y. Ma, *Appl. Phys. Lett.* **2014**, *105*, 021102.

[51] Y. Peng, X. Zang, Y. Zhu, C. Shi, L. Chen, B. Cai, S. Zhuang, *Opt. Express* **2015**, *23*, 2032.

[52] C. Gong, M. Zhan, J. Yang, Z. Wang, H. Liu, Y. Zhao, W. Liu, *Sci. Rep.* **2016**, *6*, 32466.

[53] W. Guo, Y. Liu, T. Han, *Opt. Express* **2016**, *24*, 20586.

[54] B. X. Wang, G. Z. Wang, T. Sang, L. L. Wang, *Sci. Rep.* **2017**, *7*, 41373.

[55] M. Kenney, J. Grant, Y. D. Shah, I. Escorcia-Carranza, M. Humphreys, D. R. Cumming, *ACS Photonics* **2017**, *4*, 2604.

[56] W. Zhu, F. Xiao, I. D. Rukhlenko, J. Geng, X. Liang, M. Premaratne, R. Jin, *Opt. Express* **2017**, *25*, 5781.

[57] J. Li, P. Yu, C. Tang, H. Cheng, J. Li, S. Chen, J. Tian, *Adv. Opt. Mater.* **2017**, *5*, 1700152.

[58] K. Fan, J. Y. Suen, X. Liu, W. J. Padilla, *Optica* **2017**, *4*, 601.

[59] X. Duan, S. Chen, H. Yang, H. Cheng, J. Li, W. Liu, C. Gu, J. Tian, *Appl. Phys. Lett.* **2012**, *101*, 143105.

[60] X. Duan, S. Chen, H. Cheng, Z. Li, J. Tian, *Opt. Lett.* **2013**, *38*, 483.

[61] H. Cheng, S. Chen, P. Yu, X. Duan, B. Xie, J. Tian, *Appl. Phys. Lett.* **2013**, *103*, 203112.

[62] C. Wu, N. Arju, G. Kelp, J. A. Fan, J. Dominguez, E. Gonzales, E. Tutuc, I. Brener, G. Shvets, *Nat. Commun.* **2014**, *5*, 3892.

[63] S. Campione, S. Liu, L. I. Basilio, L. K. Warne, W. L. Langston, T. S. Luk, J. R. Wendt, J. L. Reno, G. A. Keeler, I. Brener, M. B. Sinclair, *ACS Photonics* **2016**, *3*, 2362.

[64] Y. Yang, I. I. Kravchenko, D. P. Briggs, J. Valentine, *Nat. Commun.* **2014**, *5*, 5753.

[65] A. Cui, Z. Liu, J. Li, T. H. Shen, X. Xia, Z. Li, Z. Gong, H. Li, B. Wang, J. Li, H. Yang, W. Li, C. Gu, *Light: Sci. Appl.* **2015**, *4*, e308.

[66] Z. Liu, Z. Liu, J. Li, W. Li, J. Li, C. Gu, Z. Y. Li, *Sci. Rep.* **2016**, *6*, 27817.

[67] L. Cong, M. Manjappa, N. Xu, I. Al-Naib, W. Zhang, R. Singh, *Adv. Opt. Mater.* **2015**, *3*, 1537.

[68] Y. Fan, F. Zhang, N. H. Shen, Q. Fu, Z. Wei, H. Li, C. M. Soukoulis, *Phys. Rev. A* **2018**, *97*, 033816.

[69] A. A. Basharin, V. Chuguevsky, N. Volsky, M. Kafesaki, E. N. Economou, *Phys. Rev. B* **2017**, *95*, 035104.

[70] B. Luk'yanchuk, N. I. Zheludev, S. A. Maier, N. J. Halas, P. Nordlander, H. Giessen, C. T. Chong, *Nat. Mater.* **2010**, *9*, 707.

[71] M. F. Limonov, M. V. Rybin, A. N. Poddubny, Y. S. Kivshar, *Nat. Photonics* **2017**, *11*, 543.

[72] A. Tittl, A. Leitis, M. Liu, F. Yesilkoy, D. Y. Choi, D. N. Neshev, Y. S. Kivshar, H. Altug, *Science* **2018**, *360*, 1105.

[73] Y. Zhang, W. Liu, Z. Li, Z. Li, H. Cheng, S. Chen, J. Tian, *Opt. Lett.* **2018**, *43*, 1842.

[74] L. Ding, Q. Y. S. Wu, J. H. Teng, *Laser Photonics Rev.* **2014**, *8*, 941.

[75] X. L. Hu, L. B. Sun, Q. J. Wu, L. S. Wang, S. A. Bai, Q. Li, S. M. Yang, R. Z. Tai, M. Mohr, H. J. Fecht, L. Q. Wang, D. X. Zhang, J. Z. Jiang, *J. Appl. Phys.* **2017**, *121*, 153105.

[76] L. Huang, C. C. Chang, B. Zeng, J. Nogan, S. N. Luo, A. J. Taylor, A. K. Azad, H. T. Chen, *ACS Photonics* **2017**, *4*, 2111.

[77] N. Yu, P. Genevet, , M. A. Kats, F. Aieta, J. P. Tetienne, F. Capasso, Z. Gaburro, *Science* **2011**, *334*, 333.

[78] M. A. Kats, P. Genevet, G. Aoust, N. Yu, R. Blanchard, F. Aieta, Z. Gaburro, F. Capasso, *Proc. Natl. Acad. Sci. USA* **2012**, *109*, 12364.

[79] F. Aieta, P. Genevet, M. A. Kats, N. Yu, R. Blanchard, Z. Gaburro, F. Capasso, *Nano Lett.* **2012**, *12*, 4932.

[80] Z. Zhao, M. Pu, H. Gao, J. Jin, X. Li, X. Ma, Y. Wang, P. Gao, X. Luo, *Sci. Rep.* **2015**, *5*, 15781.

[81] C. Pfeiffer, A. Grbic, *Phys. Rev. Lett.* **2016**, *117*, 077401.

[82] Z. Liu, S. Chen, J. Li, H. Cheng, Z. Li, W. Liu, P. Yu, J. Xia, J. Tian, *Opt. Lett.* **2014**, *39*, 6763.

[83] H. Cheng, S. Chen, P. Yu, W. Liu, Z. Li, J. Li, B. Xie, J. Tian, *Adv. Opt. Mater.* **2015**, *3*, 1744.

[84] Z. Li, W. Liu, H. Cheng, J. Liu, S. Chen, J. Tian, *Sci. Rep.* **2016**, *6*, 35485.

[85] J. Liu, Z. Li, W. Liu, H. Cheng, S. Chen, J. Tian, *Adv. Opt. Mater.* **2016**, *4*, 2028.

[86] H. Cheng, X. Wei, P. Yu, Z. Li, Z. Liu, J. Li, S. Chen, J. Tian, *Appl. Phys. Lett.* **2017**, *110*, 171903.

[87] Y. Wang, M. Pu, Z. Zhang, X. Li, X. Ma, Z. Zhao, X. Luo, *Sci. Rep.* **2016**, *5*, 17733.

[88] Z. E. Bomzon, V. Kleiner, E. Hasman, *Opt. Lett.* **2001**, *26*, 1424.

[89] Z. E. Bomzon, G. Biener, V. Kleiner, E. Hasman, *Opt. Lett.* **2002**, *27*, 1141.

[90] X. Chen, L. Huang, H. Mühlenbernd, G. Li, B. Bai, Q. Tan, G. Jin, C.-W. Qiu, S. Zhang, T. Zentgraf, *Nat. Commun.* **2012**, *3*, 1198.

[91] Z. Liu, Z. Li, Z. Liu, J. Li, H. Cheng, P. Yu, W. Liu, C. Tang, C. Gu, J. Li, S. Chen, J. Tian, *Adv. Funct. Mater.* **2015**, *25*, 5428.

[92] J. Li, N. Verellen, P. V. Dorpe, *ACS Photonics* **2017**, *4*, 1893.

[93] S. Liu, A. Vaskin, S. Campione, O. Wolf, M. B. Sinclair, J. Reno, G. A. Keeler, I. Staude, I. Brener, *Nano Lett.* **2017**, *17*, 4297.

[94] M. Decker, I. Staude, M. Falkner, J. Dominguez, D. N. Neshev, I. Brener, T. Pertsch, Y. S. Kivshar, *Adv. Opt. Mater.* **2015**, *3*, 813.

[95] S. Qi, Y. Li, B. Assouar, *Phys. Rev. Lett.* **2017**, *7*, 054006.

[96] E. Arbabi, A. Arbabi, S. M. Kamali, Y. Horie, A. Faraon, *Optica* **2016**, *3*, 628.

[97] M. Khorasaninejad, W. T. Chen, A. Y. Zhu, J. Oh, R. C. Devlin, D. Rousso, F. Capasso, *Nano Lett.* **2016**, *16*, 4595.

[98] M. Khorasaninejad, W. T. Chen, R. C. Devlin, J. Oh, A. Y. Zhu, F. Capasso, *Science* **2016**, *352*, 1190.

[99] A. Arbabi, E. Arbabi, S. M. Kamali, Y. Horie, S. Han, A. Faraon, *Nat. Commun.* **2016**, *7*, 13682.

[100] L. Cong, W. Cao, X. Zhang, Z. Tian, J. Gu, R. Singh, J. Han, W. Zhang, *Appl. Phys. Lett.* **2013**, *103*, 171107.

[101] L. Cong, N. Xu, J. Han, W. Zhang, R. Singh, *Adv. Mater.* **2015**, *27*, 6630.

[102] L. Cong, N. Xu, J. Gu, R. Singh, J. Han, W. Zhang, *Laser Photonics Rev.* **2014**, *8*, 626.

[103] F. Aieta, M. A. Kats, P. Genevet, F. Capasso, *Science* **2015**, *347*, 1342.

[104] M. Khorasaninejad, F. Aieta, P. Kanhaiya, M. A. Kats, P. Genevet, D. Rousso, F. Capasso, *Nano Lett.* **2015**, *15*, 5358.

[105] M. Khorasaninejad, Z. Shi, A. Y. Zhu, W. T. Chen, V. Sanjeev, A. Zaidi, F. Capasso, *Nano Lett.* **2017**, *17*, 1819.

[106] M. Khorasaninejad, F. Capasso, *Science* **2017**, *358*, eaam8100.

[107] S. Wang, J. Lai, T. Wu, X. Li, J. Sun, *J. Phys. D: Appl. Phys.* **2017**, *50*, 455101.

[108] O. Avayu, E. Almeida, Y. Prior, T. Ellenbogen, *Nat. Commun.* **2017**, *8*, 14992.

[109] S. Wang, P. C. Wu, V. C. Su, Y. C. Lai, C. H. Chu, J. W. Chen, S. H. Lu, J. Chen, B. Xu, C. H. Kuan, T. Li, S. Zhu, D. P. Tsai, *Nat. Commun.* **2017**, *8*, 187.

[110] Q. Wei, L. Huang, X. Li, J. Liu, Y. Wang, *Adv. Opt. Mater.* **2017**, *5*, 1700434.

[111] S. Larouche, Y. J. Tsai, T. Tyler, N. M. Jokerst, D. R. Smith, *Nat. Mater.* **2012**, *11*, 450.

[112] L. Li, T. J. Cui, W. Ji, S. Liu, J. Ding, X. Wan, Y. B. Li, M. Jiang, C.-W. Qiu, S. Zhang, *Nat. Commun.* **2017**, *8*, 197.

[113] B. Wang, F. Dong, Q. T. Li, D. Yang, C. Sun, J. Chen, Z. Song, L. Xu, W. Chu, Y. F. Xiao, Q. Gong, Y. Li, *Nano Lett.* **2016**, *16*, 5235.

[114] M. Khorasaninejad, A. Ambrosio, P. Kanhaiya, F. Capasso, *Sci. Adv.* **2016**, *2*, e1501258.

[115] T. Li, H. Liu, S. M. Wang, X. G. Yin, F. M. Wang, S. N. Zhu, X. Zhang, *Appl. Phys. Lett.* **2008**, *93*, 021110.

[116] R. Gordon, A. G. Brolo, A. McKinnon, A. Rajora, B. Leathem, K. L. Kavanagh, *Phys. Rev. Lett.* **2004**, *92*, 037401.

[117] Y. Zhao, A. Alù, *Nano Lett.* **2013**, *13*, 1086.

[118] A. Pors, M. G. Nielsen, G. Della Valle, M. Willatzen, O. Albrektsen, S. I. Bozhevolnyi, *Opt. Lett.* **2011**, *36*, 1626.

[119] Z. Li, W. Liu, H. Cheng, S. Chen, J. Tian, *Sci. Rep.* **2016**, *5*, 18106.

[120] Z. Li, S. Chen, W. Liu, H. Cheng, Z. Liu, J. Li, P. Yu, B. Xie, J. Tian, *Plasmonics* **2015**, *10*, 1703.

[121] Z. Liu, Z. Li, Z. Liu, H. Cheng, W. Liu, C. Tang, C. Gu, J. Li, H.-T. Chen, S. Chen, J. Tian, *ACS Photonics* **2017**, *4*, 2061.

[122] W. Liu, S. Chen, Z. Li, H. Cheng, P. Yu, J. Li, J. Tian, *Opt. Lett.* **2015**, *40*, 3185.

[123] S. Wu, Z. Zhang, Y. Zhang, K. Zhang, L. Zhou, X. Zhang, Y. Zhu, *Phys. Rev. Lett.* **2013**, *110*, 207401.

[124] N. Yu, F. Aieta, P. Genevet, M. A. Kats, Z. Gaburro, F. Capasso, *Nano Lett.* **2012**, *12*, 6328.

[125] P. Yu, J. Li, C. Tang, H. Cheng, Z. Liu, Z. Li, Z. Liu, C. Gu, J. Li, S. Chen, J. Tian, *Light: Sci. Appl.* **2016**, *5*, e16096.

[126] Z. Li, W. Liu, H. Cheng, S. Chen, J. Tian, *Adv. Opt. Mater.* **2017**, *5*, 1700413.

[127] Z. Li, W. Liu, H. Cheng, S. Chen, J. Tian, *Sci. Rep.* **2017**, *7*, 8204.

[128] S. Chen, W. Liu, Z. Li, H. Cheng, J. Tian, *Metamaterials—Devices and Advanced Applications*, IN-TECH, London, UK **2016**.

[129] J. Li, P. Yu, H. Cheng, W. Liu, Z. Li, B. Xie, S. Chen, J. Tian, *Adv. Opt. Mater.* **2016**, *4*, 91.

[130] Z. Li, W. Liu, H. Cheng, S. Chen, J. Tian, *Opt. Lett.* **2016**, *41*, 3142.

[131] H. Cheng, S. Chen, P. Yu, J. Li, B. Xie, Z. Li, J. Tian, *Appl. Phys. Lett.* **2013**, *103*, 223102.

[132] H Cheng, S. Chen, P. Yu, J. Li, L. Deng, J. Tian, *Opt. Lett.* **2013**, *38*, 1567.

[133] N. K. Grady, J. E. Heyes, D. R. Chowdhury, Y. Zeng, M. T. Reiten, A. K. Azad, A. J. Taylor, D. A. R. Dalvit, H.-T. Chen, *Science* **2013**, *340*, 1304.

[134] Z. Li, G. Zheng, P. A. He, S. Li, Q. Deng, J. Zhao, Y. Ai, *Opt. Lett.* **2015**, *40*, 4285.

[135] Y. Yang, W. Wang, P. Moitra, I. I. Kravchenko, D. P. Briggs, J. Valentine, *Nano Lett.* **2014**, *14*, 1394.

[136] M. Khorasaninejad, K. B. Crozier, *Nat. Commun.* **2014**, *5*, 5386.

[137] S. Kruk, B. Hopkins, I. I. Kravchenko, A. Miroshnichenko, D. N. Neshev, Y. S. Kivshar, *APL Photonics* **2016**, *1*, 030801.

[138] H. Suchowski, K. O'Brien, Z. J. Wong, A. Salandrino, X. Yin, X. Zhang, *Science* **2013**, *342*, 1223.

[139] J. Butet, P. F. Brevet, O. J. Martin, *ACS Nano* **2015**, *9*, 10545.

[140] M. W. Klein, C. Enkrich, M. Wegener, S. Linden, *Science* **2006**, *313*, 502.

[141] S. Linden, F. B. P. Niesler, J. Förstner, Y. Grynko, T. Meier, M. Wegener, *Phys. Rev. Lett.* **2012**, *109*, 015502.

[142] B. Metzger, L. Gui, J. Fuchs, D. Floess, M. Hentschel, H. Giessen, *Nano Lett.* **2015**, *15*, 3917.

[143] H. Linnenbank, S. Linden, *Optica* **2015**, *2*, 698.

[144] S. D. Liu, E. S. P. Leong, G. C. Li, Y. Hou, J. Deng, J. H. Teng, H. C. Ong, D. Y. Lei, *ACS Nano* **2016**, *10*, 1442.

[145] K. Thyagarajan, S. Rivier, A. Lovera, O. J. Martin, *Opt. Express* **2012**, *20*, 12860.

[146] H. Aouani, M. Navarro-Cia, M. Rahmani, T. P. Sidiropoulos, M. Hong, R. F. Oulton, S. A. Maier, *Nano Lett.* **2012**, *12*, 4997.

[147] M. Celebrano, X. Wu, M. Baselli, S. Großmann, P. Biagioni, A. Locatelli, C. D. Angelis, G. Cerullo, R. Osellame, B. Hecht, L. Duò, F. Ciccacci, M. Finazzi, *Nat. Nanotechnol.* **2015**, *10*, 412.

[148] G. Grinblat, Y. Li, M. P. Nielsen, R. F. Oulton, S. A. Maier, *Nano Lett.* **2016**, *16*, 4635.

[149] M. R. Shcherbakov, D. N. Neshev, B. Hopkins, A. S. Shorokhov, I. Staude, E. V. Melik-Gaykazyan, M. Decker, A. A. Ezhov, A. E. Miroshnichenko, I. Brener, A. A. Fedyanin, Y. S. Kivshar, *Nano Lett.* **2014**, *14*, 6488.

[150] L. Wang, S. Kruk, L. Xu, M. Rahmani, D. Smirnova, A. Solntsev, I. Kravchenko, D. Neshev, Y. Kivshar, *Nanoscale* **2017**, *9*, 2201.

[151] A. S. Shorokhov, E. V. Melik-Gaykazyan, D. A. Smirnova, B. Hopkins, K. E. Chong, D.-Y. Choi, M. R. Shcherbakov, A. E. Biroshnichenko, D. N. Neshev, A. A. Fedyanin, Y. S. Kivshar, *Nano Lett.* **2016**, *16*, 4857.

[152] W. Tong, C. Gong, X. Liu, S. Yuan, Q. Huang, J. Xia, Y. Wang, *Opt. Express* **2016**, *24*, 19661.

[153] Y. Yang, W. Wang, A. Boulesbaa, I. I. Kravchenko, D. P. Briggs, A. Puretzky, D. Geohegan, J. Valentine, *Nano Lett.* **2015**, *15*, 7388.

[154] J. Renger, R. Quidant, N. Van Hulst, L. Novotny, *Phys. Rev. Lett.* **2010**, *104*, 046803.

[155] B. Simkhovich, G. Bartal, *Phys. Rev. Lett.* **2014**, *112*, 056802.

[156] G. Vampa, B. G. Ghamsari, S. S. Mousavi, T. J. Hammond, A. Olivieri, E. Lisicka-Skrek, A. Yu Naumov, D. M. Villeneuve, A. Staudte, P. Berini, P. B. Corkum, *Nat. Phys.* **2017**, *13*, 659.

[157] J. Lee, N. Nookala, J. S. Gomez-Diaz, M. Tymchenko, F. Demmerle, G. Boehm, M. C. Amann, A. Alù, M. A. Belkin, *Adv. Opt. Mater.* **2016**, *4*, 664.

[158] Z. Li, W. Liu, Z. Li, H. Cheng, S. Chen, J. Tian, *Opt. Lett.* **2017**, *42*, 3117.

[159] J. Lee, M. Tymchenko, C. Argyropoulos, P. Y. Chen, F. Lu, F. Demmerle, G. Boehm, M.-C. Amann, A. Alù, M. A. Belkin *Nature* **2014**, *511*, 65.

[160] C. Huang, C. Zhang, J. Yang, B. Sun, B. Zhao, X. Luo, *Adv. Opt. Mater.* **2017**, *5*, 1700485.

[161] P. C. Wu, W. Zhu, Z. X. Shen, P. H. J. Chong, W. Ser, D. P. Tsai, A. Q. Liu, *Adv. Opt. Mater.* **2017**, *5*, 1600938.

[162] S. Aksu, M. Huang, A. Artar, A. A. Yanik, S. Selvarasah, M. R. Dokmeci, H. Altug, *Adv. Mater.* **2011**, *23*, 4422.

[163] M. Manjappa, Y. K. Srivastava, L. Cong, I. Al-Naib, R. Singh, *Adv. Mater.* **2017**, *29*, 1603355.

[164] L. Cong, Y. K. Srivastava, A. Solanki, T. C. Sum, R. Singh, *ACS Photonics* **2017**, *4*, 1595.

[165] Y. K. Srivastava, M. Manjappa, L. Cong, H. N. Krishnamoorthy, V. Savinov, P. Pitchappa, R. Singh, *Adv. Mater.* **2018**, *30*, 1801257.

[166] M. Gupta, Y. K. Srivastava, R. Singh, *Adv. Mater.* **2018**, *30*, 1704845.

[167] W. X. Lim, M. Manjappa, Y. K. Srivastava, L. Cong, A. Kumar, K. F. MacDonald, R. Singh, *Adv. Mater.* **2018**, *30*, 1705331.

[168] J. Y. Ou, E. Plum, L. Jiang, N. I. Zheludev, *Nano Lett.* **2011**, *11*, 2142.

[169] N. K. Emani, T. F. Chung, X. Ni, A. V. Kildishev, Y. P. Chen, A. Boltasseva, *Nano Lett.* **2012**, *12*, 5202.

[170] X. Yin, T. Steinle, L. Huang, T. Taubner, M. Wuttig, T. Zentgraf, H. Giessen, *Light: Sci. Appl.* **2017**, *6*, e17016.

[171] C. H. Chu, M. L. Tseng, J. Chen, P. C. Wu, Y. H. Chen, H. C. Wang, T. Y. Chen, W. T. Hsieh, H. J. Wu, G. Sun, D. P. Tsai, *Laser Photonics Rev.* **2016**, *10*, 986.

[172] Z. Y. Jia, F. Z. Shu, Y. J. Gao, F. Cheng, R. W. Peng, R. H. Fan, Y. Liu, M. Wang, *Phys. Rev. Appl.* **2018**, *9*, 034009.

[173] G. Li, T. Zentgraf, S. Zhang, *Nat. Phys.* **2016**, *12*, 736.

[174] K. F. Li, J. H. Deng, X. Liu, G. Li, *Laser Photonics Rev.* **2018**, *12*, 1700204.

[175] P. Georgi, C. Schlickriede, G. Li, S. Zhang, T. Zentgraf, *Optica* **2017**, *4*, 1000.

[176] K. Melde, A. G. Mark, T. Qiu, P. Fischer, *Nature* **2016**, *537*, 518.

[177] Q. Xu, X. Zhang, Y. Xu, C. Ouyang, Z. Tian, J. Gu, J. Li, S. Zhang, J. Han, W. Zhang, *Laser Photonics Rev.* **2017**, *11*, 1600212.

[178] L. Huang, H. Mühlenbernd, X. Li, X. Song, B. Bai, Y. Wang, T. Zentgraf, *Adv. Mater.* **2015**, *27*, 6444.

[179] W. Zhao, H. Jiang, B. Liu, J. Song, Y. Jiang, C. Tang, J. Li, *Sci. Rep.* **2016**, *6*, 30613.

[180] D. Wen, F. Yue, G. Li, G. Zheng, K. Chan, S. Chen, M. Chen, K. F. Li, P. W. H. Wong, K. W. Cheah, E. Y. B. Pun, S. Zhang, X. Chen, *Nat. Commun.* **2015**, *6*, 8241.

[181] G. Minatti, F. Caminita, E. Martini, M. Sabbadini, S. Maci, *IEEE Trans. Antennas Propag.* **2016**, *64*, 3907.

[182] A. Pors, S. I. Bozhevolnyi, *Opt. Mater. Express* **2015**, *5*, 2448.

[183] H. Mühlenbernd, P. Georgi, N. Pholchai, L. Huang, G. Li, S. Zhang, T. Zentgraf, *ACS Photonics* **2016**, *3*, 124.

[184] W. Liu, Z. Li, H. Cheng, S. Chen, J. Tian, *Phys. Rev. Appl.* **2017**, *8*, 014012.

[185] M. Kim, A. M. Wong, G. V. Eleftheriades, *Phys. Rev. X* **2014**, *4*, 041042.

[186] X. Zhang, Z. Tian, W. Yue, J. Gu, S. Zhang, J. Han, W. Zhang, *Adv. Mater.* **2013**, *25*, 4567.

[187] L. Liu, X. Zhang, M. Kenney, X. Su, N. Xu, C. Ouyang, Y. Shi, J. Han, W. Zhang, S. Zhang, *Adv. Mater.* **2014**, *26*, 5031.

[188] Z. Li, H. Cheng, Z. Liu, S. Chen, J. Tian, *Adv. Opt. Mater.* **2016**, *4*, 1230.

[189] G. Y. Lee, G. Yoon, S. Y. Lee, H. Yun, J. Cho, K. Lee, H. Kim, J. Rho, B. Lee, *Nanoscale* **2018**, *10*, 4237.

[190] H. Wang, L. Shi, B. Lukyanchuk, C. Sheppard, C. T. Chong, *Nat. Photonics* **2008**, *2*, 501.

[191] E. T. Rogers, J. Lindberg, T. Roy, S. Savo, J. E. Chad, M. R. Dennis, N. I. Zheludev, *Nat. Mater.* **2012**, *11*, 432.

[192] K. Kitamura, K. Sakai, S. Noda, *Opt. Express* **2010**, *18*, 4518.

[193] J. Li, S. Chen, H. Yang, J. Li, P. Yu, H. Cheng, C. Gu, H.-T. Chen, J. Tian, *Adv. Funct. Mater.* **2015**, *25*, 704.

[194] P. Yu, S. Chen, J. Li, H. Cheng, Z. Li, W. Liu, B. Xie, Z. Liu, J. Tian, *Opt. Lett.* **2015**, *40*, 3229.

[195] J. B. Mueller, N. A. Rubin, R. C. Devlin, B. Groever, F. Capasso, *Phys. Rev. Lett.* **2017**, *118*, 113901.

[196] A. Arbabi, Y. Horie, M. Bagheri, A. Faraon, *Nat. Nanotechnol.* **2015**, *10*, 937.

[197] G. Biener, A. Niv, V. Kleiner, E. Hasman, *Opt. Lett.* **2002**, *27*, 1875.

[198] L. Marrucci, C. Manzo, D. Paparo, *Phys. Rev. Lett.* **2006**, *96*, 163905.

[199] D. Naidoo, F. S. Roux, A. Dudley, I. Litvin, B. Piccirillo, L. Marrucci, A. Forbes, *Nat. Photonics* **2016**, *10*, 327.

[200] E. Nagali, L. Sansoni, F. Sciarrino, F. De Martini, L. Marrucci, B. Piccirillo, E. Karimi, E. Santamato, *Nat. Photonics* **2009**, *3*, 720.

[201] R. C. Devlin, A. Ambrosio, N. A. Rubin, J. B. Mueller, F. Capasso, *Science* **2017**, *358*, 896.

[202] C. Pfeiffer, A. Grbic, *Appl. Phys. Lett.* **2013**, *102*, 231116.

[203] S. Chen, G. Li, F. Zeuner, W. H. Wong, E. Y. B. Pun, T. Zentgraf, K. W. Cheah, S. Zhang, *Phys. Rev. Lett.* **2014**, *113*, 033901.

[204] G. Li, L. Wu, K. F. Li, S. Chen, C. Schlickriede, Z. Xu, S. Huang, W.-D. Li, Y. J. Liu, E. Y.-B. Pun, T. Zentgraf, K. W. Cheah, Y. Luo, S. Zhang, *Nano Lett.* **2017**, *17*, 7974.

[205] M. K. Hedayati, M. Elbahri, *Plasmonics* **2017**, *12*, 1463.

[206] K. Kumar, H. Duan, R. S. Hegde, S. C. Koh, J. N. Wei, J. K. Yang, *Nat. Nanotechnol.* **2012**, *7*, 557.

[207] S. J. Tan, L. Zhang, D. Zhu, X. M. Goh, Y. M. Wang, K. Kumar, C.-W. Qiu, J. K. W. Yang, *Nano Lett.* **2014**, *14*, 4023.

[208] X. M. Goh, Y. Zheng, S. J. Tan, L. Zhang, K. Kumar, C. W. Qiu, J. K. Yang, *Nat. Commun.* **2014**, *5*, 5361.

[209] W. Yue, S. Gao, S. S. Lee, E. S. Kim, D. Y. Choi, *Laser Photonics Rev.* **2017**, *11*, 1600285.

[210] J. Zhao, X. Yu, X. Yang, Q. Xiang, H. Duan, Y. Yu, *Opt. Express* **2017**, *25*, 23137.

[211] T. Wood, M. Naffouti, J. Berthelot, T. David, J. B. Claude, L. Métayer, A. Delobbe, L. Favre, A. Ronda, I. Berbezier, N. Bonod, M. Abbarchi, *ACS Photonics* **2017**, *4*, 873.

[212] V. Vashistha, G. Vaidya, R. S. Hegde, A. E. Serebryannikov, N. Bonod, M. Krawczyk, *ACS Photonics* **2017**, *4*, 1076.

[213] J. Proust, F. Bedu, B. Gallas, I. Ozerov, N. Bonod, *ACS Nano* **2016**, *10*, 7761.

**ADVANCED
SCIENCE NEWS**

www.advancedsciencenews.com

**ADVANCED
MATERIALS**

www.advmat.de

[214] S. Sun, Z. Zhou, C. Zhang, Y. Gao, Z. Duan, S. Xiao, Q. Song, *ACS Nano* **2017**, *11*, 4445.

[215] V. Flauraud, M. Reyes, R. Paniagua-Dominguez, A. I. Kuznetsov, J. Brugger, *ACS Photonics* **2017**, *4*, 1913.

[216] T. Ellenbogen, K. Seo, K. B. Crozier, *Nano Lett.* **2012**, *12*, 1026.

[217] Y. Cui, R. S. Hegde, I. Y. Phang, H. K. Lee, X. Y. Ling, *Nanoscale* **2014**, *6*, 282.

[218] I. Koirala, V. R. Shrestha, C. S. Park, S. S. Lee, D. Y. Choi, *Sci. Rep.* **2017**, *7*, 40073.

[219] L. Duempelmann, A. Luu-Dinh, B. Gallinet, L. Novotny, *ACS Photonics* **2016**, *3*, 190.

[220] P. R. Wiecha, A. Arbouet, C. Girard, A. Lecestre, G. Larrieu, V. Paillard, *Nat. Nanotechnol.* **2017**, *12*, 163.

[221] S. Chen, F. Zeuner, M. Weismann, B. Reineke, G. Li, V. K. Valev, K. W. Cheah, N. C. Panoiu, T. Zentgraf, S. Zhang, *Adv. Mater.* **2016**, *28*, 2992.

[222] S. P. Rodrigues, S. Lan, L. Kang, Y. Cui, W. Cai, *Adv. Mater.* **2014**, *26*, 6157.

[223] F. Walter, G. Li, C. Meier, S. Zhang, T. Zentgraf, *Nano Lett.* **2017**, *17*, 3171.

[224] G. Li, S. Chen, N. Pholchai, B. Reineke, P. W. H. Wong, E. Y. B. Pun, K. W. Cheah, T. Zentgraf, S. Zhang, *Nat. Mater.* **2015**, *14*, 607.

[225] N. Segal, S. Keren-Zur, N. Hendler, T. Ellenbogen, *Nat. Photonics* **2015**, *9*, 180.

[226] E. Almeida, G. Shalem, Y. Prior, *Nat. Commun.* **2016**, *7*, 10367.

[227] M. Tymchenko, J. S. Gomez-Diaz, J. Lee, N. Nookala, M. A. Belkin, A. Alù, *Phys. Rev. B* **2016**, *94*, 214303.

[228] N. Nookala, J. Lee, M. Tymchenko, J. S. Gomez-Diaz, F. Demmerle, G. Boehm, K. Lai, G. Shvets, M.-C. Amann, A. Alù, M. Belkin, *Optica* **2016**, *3*, 283.

[229] W. Ye, X. Li, J. Liu, S. Zhang, *Opt. Express* **2016**, *24*, 25805.

[230] S. Keren-Zur, O. Avayu, L. Michaeli, T. Ellenbogen, *ACS Photonics* **2016**, *3*, 117.

[231] E. Almeida, O. Bitton, Y. Prior, *Nat. Commun.* **2016**, *7*, 12533.

[232] W. Ye, F. Zeuner, X. Li, B. Reineke, S. He, C. W. Qiu, T. Zentgraf, *Nat. Commun.* **2016**, *7*, 11930.

[233] P. Cheben, R. Halir, J. H. Schmid, H. A. Atwater, D. R. Smith, *Nature* **2018**, *560*, 565.

[234] W. Liu, Z. Li, H. Cheng, C. Tang, J. Li, S. Zhang, S. Chen, J. Tian, *Adv. Mater.* **2018**, *30*, 1706368.

[235] R. Zuo, W. Liu, H. Cheng, S. Chen, J. Tian, *Adv. Opt. Mater.* **2018**, *6*, 1800795.

[236] W. Ma, F. Cheng, Y. M. Liu, *ACS Nano* **2018**, *12*, 6326.

[237] J. A. Nichols, H. W. H. Chan, M. A. B. Baker, *Biophys. Rev.* **2018**, https://doi.org/10.1007/s12551-018-0449-9.

[238] A. B. Khanikaev, G. Shvets, *Nat. Photonics* **2017**, *11*, 763.

[239] H. Zhou, C. Peng, Y. Yoon, C. W. Hsu, K. A. Nelson, L. Fu, J. D. Joannopoulos, M. Soljačić, B. Zhen, *Science* **2018**, *359*, 1009.

[240] G. Sartorello, N. Olivier, J. Zhang, W. Yue, D. J. Gosztola, G. P. Wiederrecht, G. Wurtz, A. V. Zayats, *ACS Photonics* **2016**, *3*, 1517.

[241] T. Stav, A. Faerman, E. Maguid, D. Oren, V. Kleiner, E. Hasman, M. Segev, *Science* **2018**, *361*, 1101.

[242] T. Zang, H. Luo, Y. Wang, L. Wang, Y. Lu, P. Wang, *Opt. Lett.* **2018**, *43*, 3782.

[243] K. Wu, P. Coquet, Q. J. Wang, P. Genevet, *Nat. Commun.* **2018**, *9*, 3494.

[244] H. Xu, Y. Shi, *Laser Photonics Rev.* **2018**, *12*, 1800094.

[245] Z. Li, M.-H. Kim, C. Wang, Z. Han, S. Sharstha, A. C. Overvig, M. Lu, A. Stein, A. M. Agarwal, M. Lončar, N. Yu, *Nat. Nanotechnol.* **2017**, *12*, 675.